

Supporting Information for

## Acid-catalyzed proton exchange as a novel approach for relaxivity enhancement in Gd-HPDO3A-like complexes.

Loredana Leone,<sup>a</sup> Mariangela Boccalon,<sup>b</sup> Giuseppe Ferrauto,<sup>c</sup> István Fábián,<sup>d</sup> Zsolt Baranyai,<sup>\*b</sup> Lorenzo Tei<sup>\*a</sup>

<sup>a</sup> Department of Science and Technological Innovation, Università del Piemonte Orientale, Viale T. Michel 11, 15121, Alessandria, Italy

<sup>b</sup> Bracco Imaging spa, Bracco Research Centre, Via Ribes 5, 10010 Colletterto Giacosa (TO), Italy

<sup>c</sup> Department of Molecular Biotechnology and Health Science, University of Turin, Via Nizza 52, 10126 Torino, Italy

<sup>d</sup> Department of Inorganic and Analytical Chemistry, and MTA-DE Redox and Homogeneous Catalytic Reaction Mechanisms Research Group, University of Debrecen, H-4032 Debrecen, Egyetem tér 1., Hungary

### Corresponding Authors:

#### Zsolt Baranyai

Bracco Imaging – CRB/Trieste,  
Area Science Park. Ed. Q, SS 14, km 163.5, I-34149, Basovizza Trieste, Italy.  
tel. +39 040375-7842  
fax +39 0403757831  
email: [zsolt.baranyai@bracco.com](mailto:zsolt.baranyai@bracco.com)

#### Lorenzo Tei

Department of Science and Technological Innovation, Università del Piemonte Orientale, Viale T. Michel 11, 15121, Alessandria, Italy  
tel. +39 0131360208  
fax +39 0131360250  
email: [lorenzo.tei@uniupo.it](mailto:lorenzo.tei@uniupo.it)

### Table of Content:

<b>I. Synthesis</b>	pag. 2
<b>II. Protonation and complexation equilibria of HPADO3A ligands</b>	pag. 5
<b>III. Kinetic inertness of the Gd(HPADO3A) complex</b>	pag. 11
<b>IV. Effect of NH<sub>4</sub>Cl on the proton exchange processes of Gd(HPADO3A), Gd(BzHPADO3A) and Gd(PipHPADO3A) complexes</b>	pag. 14
<b>V. Relaxometric study</b>	pag. 15
<b>VI. Chemical Exchange Saturation Transfer (CEST)-MRI study</b>	pag. 20
<b>VII. References</b>	pag. 25
<b>VIII. <sup>1</sup>H and <sup>13</sup>C NMR spectra of protected and deprotected ligands</b>	pag. 26
<b>IX. HPLC chromatograms and ESI-MS spectra of ligands and complexes</b>	pag. 32
<b>X. <sup>1</sup>H NMR spectra of EuHPADO3A</b>	pag. 41

# I. Synthesis

## I.1. Experimental

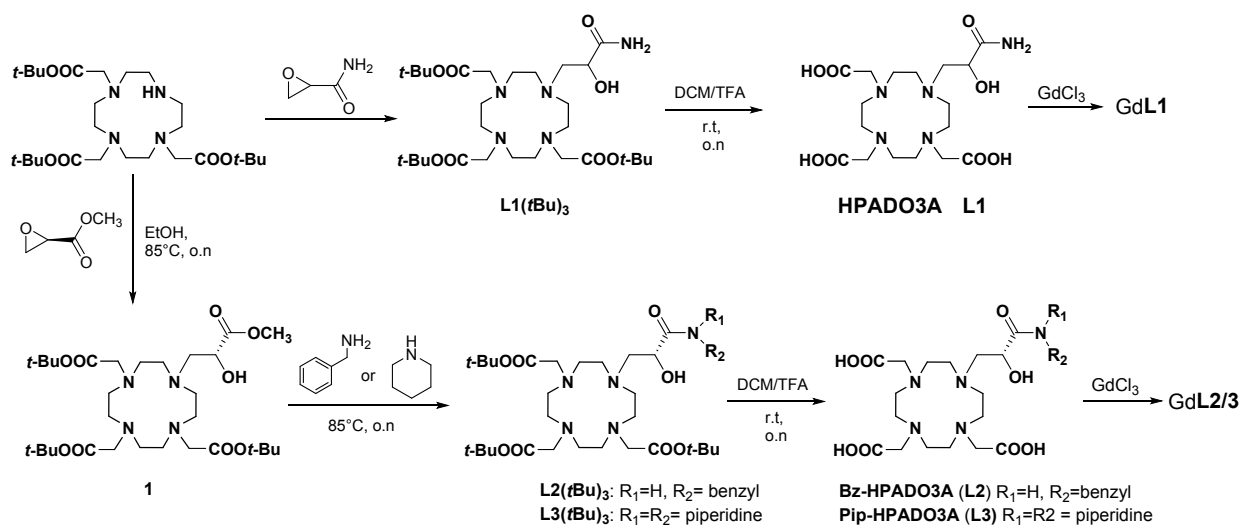
All chemicals were purchased from Sigma-Aldrich or Alfa Aesar unless otherwise stated and were used without further purification. The  $^1\text{H}$  and  $^{13}\text{C}$  NMR spectra were recorded using a Bruker Advance III 500 MHz (11.4 T) spectrometer equipped with 5mm PABBO probes and BVT-3000 temperature control unit. Chemical shifts are reported relative to TMS and were referenced using the residual proton solvent resonances. HPLC analyses and mass spectra were performed on a Waters HPLC-MS system equipped with a Waters 1525 binary pumps. Analytical measurements were carried out on a Waters Atlantis RPC18 column (5 $\mu\text{m}$  4.6x100mm) using the following methods:

Method 1: A=  $\text{H}_2\text{O}/0.1\%$  TFA; B = MeOH; flow= 1 mL/min; 0-3 min =100% A; 3-18 min = 100% B; 18-19 min = 100% B; 19-20 min = 100% A.

Semi-preparative purifications were performed on a Waters Atlantis prep T3 OBD (5 $\mu\text{m}$  19x100mm) using the following method:

Method 2: A =  $\text{H}_2\text{O}/0.1\%$  TFA; B = MeOH; flow= 20 mL/min; 0-3 min =100% A; 3-18 min = 100% B; 18-19 min = 100% B; 19-20 min = 100% A.

Electrospray ionization mass spectra (ESI MS) were recorded using a SQD 3100 Mass Detector (Waters), operating in positive or negative ion mode, with 1% v/v formic acid in methanol as the carrier solvent. High-resolution mass spectra were recorded using a high-resolution, accurate-mass (HRAM) Orbitrap detection system with a Thermo Scientific™ Q Exactive™ Orbitrap mass spectrometer.



Scheme 1S. Synthesis of Gd(HPADO3A) complexes.

## I.2. Synthesis of tri-tert-butyl 2,2',2''-(10-(3-amino-2-hydroxy-3-oxopropyl)-1,4,7,10-tetraazacyclododecane-1,4,7-triyl) triacetate (L1(*t*Bu)<sub>3</sub>)

A solution of DO3A(*t*Bu)<sub>3</sub> (103 mg, 0.2 mmol) and glycidamide (51 mg, 0.58 mmol) in *t*-BuOH (2 mL) was stirred 16 h under reflux. The solvent was removed in vacuo and then the reaction mixture was purified by silica gel chromatography (90:10  $\text{CH}_2\text{Cl}_2$ :MeOH,  $R_f$  = 0.38) to afford the protected ligand L1(*t*Bu)<sub>3</sub> (86 mg, 0.14 mmol, yield 74%).  $^1\text{H}$  NMR ( $\text{CDCl}_3$ , 500MHz):  $\delta$  (ppm)= 4.48 (m, 1H,  $-\text{NCH}_2\text{CH}(\text{OH})-$ ), 3.87-2.93 (m, macrocycle,  $-\text{NCH}_2\text{COOC}(\text{CH}_3)_3$ ,  $-\text{NCH}_2\text{CH}(\text{OH})-$ , 24H), 1.45-1.51 (s, 27H,  $-\text{NCH}_2\text{COOC}(\text{CH}_3)_3$ );  $^{13}\text{C}$  NMR ( $\text{CDCl}_3$ , 125MHz):  $\delta$ = 174.6 ( $-\text{CH}_2\text{CO}-\text{NH}_2$ ), 171.3 ( $-\text{NCH}_2\text{COOC}(\text{CH}_3)_3$ ), 85.9-84.6 ( $-\text{C}(\text{CH}_3)_3$ ), 67.5 ( $-\text{NCH}_2\text{CH}(\text{OH})-$ ), 57.1 ( $-\text{NCH}_2\text{CH}(\text{OH})-$ ), 56.2 ( $-\text{NCH}_2\text{COOC}(\text{CH}_3)_3$ ), 55.4-

50.4 (macrocycle), 28.9 (-C(CH<sub>3</sub>)<sub>3</sub>). ESI-MS (m/z): found 602.89 (M+H<sup>+</sup>) (calc for C<sub>29</sub>H<sub>56</sub>N<sub>5</sub>O<sub>8</sub>:602.79).

### I.3. Synthesis of tri-tert-butyl 2,2',2''-(10-(2-hydroxy-3-methoxy-3-oxopropyl)-1,4,7,10-tetraazacyclododecane-1,4,7-triyl) triacetate (**1**)

A solution of DO3A(*t*Bu)<sub>3</sub> (103 mg, 0.2 mmol) and (*R*)-methylglycidate (86  $\mu$ l, 2 mmol) in *t*-BuOH (2 mL) was stirred for 16 hours under reflux. The solvent was removed in vacuo and then the reaction mixture was purified by silica gel chromatography (90:10 CH<sub>2</sub>Cl<sub>2</sub>:MeOH, R<sub>f</sub> = 0.45) to afford compound **1** (111 mg, 0.16 mmol, yield 80%). <sup>1</sup>H NMR (CDCl<sub>3</sub>, 500MHz):  $\delta$ = 1.45 (s, 27H, -NCH<sub>2</sub>COOC(CH<sub>3</sub>)<sub>3</sub>), 3.68-3.17 (m, macrocycle, -NCH<sub>2</sub>COOC(CH<sub>3</sub>)<sub>3</sub>, 22H), 3.70 (s, 3H, -OCH<sub>3</sub>), 9H, 4.11 (m, 2H, -NCH<sub>2</sub>CH(OH)-), 4.38 (m, 1H, -NCH<sub>2</sub>CH(OH)-) <sup>13</sup>C NMR (CDCl<sub>3</sub>, 125MHz):  $\delta$ = 170.1 (-CH<sub>2</sub>COOCH<sub>3</sub>), 169.5 (-NCH<sub>2</sub>COOC(CH<sub>3</sub>)<sub>3</sub>), 82.0 (-C(CH<sub>3</sub>)<sub>3</sub>), 78.3 (-NCH<sub>2</sub>CH(OH)-), 58.8 (-NCH<sub>2</sub>CH(OH)-), 57.4 (-NCH<sub>2</sub>COOC(CH<sub>3</sub>)<sub>3</sub>), 53.2 (-OCH<sub>3</sub>), 48.7-52.1 (macrocycle), 27.8 (-C(CH<sub>3</sub>)<sub>3</sub>). ESI-MS (m/z): found 617.71 (M+H<sup>+</sup>) (calc for C<sub>30</sub>H<sub>57</sub>N<sub>4</sub>O<sub>9</sub>:617.81).

### I.4. Synthesis of tri-tert-butyl 2,2',2''-(10-(3-(benzylamino)-2-hydroxy-3-oxopropyl)-1,4,7,10-tetraazacyclododecane-1,4,7-triyl) triacetate (**L2**(*t*Bu)<sub>3</sub>)

Compound **1** (50 mg, 0.081 mmol) was dissolved in benzylamine (2 ml) and the reaction was stirred for 16 hours at 70°C. The reaction mixture was washed with water, solvent was evaporated in vacuo and then purified by silica gel chromatography (90:10 CH<sub>2</sub>Cl<sub>2</sub>:MeOH, R<sub>f</sub> = 0.52) to afford **L2**(*t*Bu)<sub>3</sub> (36 mg, 0.053 mmol, yield 65%). <sup>1</sup>H NMR (CDCl<sub>3</sub>, 500MHz):  $\delta$ = 7.38-7.31 (m, *Ph*, 5H), 4.71 (m, 1H, -NCH<sub>2</sub>CH(OH)-), 4.47 (m, 2H, -CH<sub>2</sub>Ph), 4.06-2.98 (m, macrocycle, -NCH<sub>2</sub>COOC(CH<sub>3</sub>)<sub>3</sub>, -NCH<sub>2</sub>CH(OH)-, 24H), 1.57-1.46 (s, 27 H, -NCH<sub>2</sub>COOC(CH<sub>3</sub>)<sub>3</sub>). <sup>13</sup>C NMR (CDCl<sub>3</sub>, 125MHz):  $\delta$ = 170.7 (-CH<sub>2</sub>CO-NHCH<sub>2</sub>Ph), 170.0 (-NCH<sub>2</sub>COOC(CH<sub>3</sub>)<sub>3</sub>), 137.4 (Ph-*ipso*), 128.7 (Ph-*meta*), 127.7 (Ph-*ortho*), 127.6 (Ph-*para*), 85.0-84.6 (-C(CH<sub>3</sub>)<sub>3</sub>), 66.5 (-NCH<sub>2</sub>CH(OH)-), 56.0 (-NCH<sub>2</sub>CH(OH)-), 54.9-54.1 (-NCH<sub>2</sub>COOC(CH<sub>3</sub>)<sub>3</sub>), 51.5-49.1 (macrocycle), 43.5 (-CH<sub>2</sub>Ph), 27.9-27.8 (-NCH<sub>2</sub>COOC(CH<sub>3</sub>)<sub>3</sub>). ESI-MS (m/z): found 692.81 (M+H<sup>+</sup>) (calc for C<sub>36</sub>H<sub>62</sub>N<sub>5</sub>O<sub>8</sub>:692.92).

### I.5. Synthesis of tri-tert-butyl 2,2',2''-(10-(2-hydroxy-3-oxo-3-(piperidin-1-yl)propyl)-1,4,7,10-tetraazacyclododecane-1,4,7-triyl) triacetate (**L3**(*t*Bu)<sub>3</sub>)

Compound **1** (100 mg, 0.162 mmol) was dissolved in piperidine (2 ml) and the reaction was stirred for 16 hours at 70°C. The solvent was evaporated in vacuo and then purified by silica gel chromatography (90:10 CH<sub>2</sub>Cl<sub>2</sub>:MeOH, R<sub>f</sub> = 0.60) to afford **L3**(*t*Bu)<sub>3</sub> (54 mg, 0.081 mmol, yield 50%). <sup>1</sup>H NMR (CDCl<sub>3</sub>, 500MHz):  $\delta$ = 4.01 (m, 1H, -NCH<sub>2</sub>CH(OH)-), 3.94-2.91 (m, macrocycle, -NCH<sub>2</sub>COOC(CH<sub>3</sub>)<sub>3</sub>, -NCH<sub>2</sub>CH(OH)-, -NCH<sub>2</sub>(CH<sub>2</sub>)<sub>3</sub>-, 28H), 1.81-1.40 (s, 27 H, -NCH<sub>2</sub>COOC(CH<sub>3</sub>)<sub>3</sub>; m, 6H, -NCH<sub>2</sub>(CH<sub>2</sub>)<sub>3</sub>-). <sup>13</sup>C NMR (CDCl<sub>3</sub>, 125MHz):  $\delta$ = 170.2 (-CH<sub>2</sub>CO-NH-), 167.7 (-NCH<sub>2</sub>COOC(CH<sub>3</sub>)<sub>3</sub>), 84.8 (-C(CH<sub>3</sub>)<sub>3</sub>), 62.3 (-NCH<sub>2</sub>CH(OH)-), 55.0 (-NCH<sub>2</sub>CH(OH)-), 54.1 (-NCH<sub>2</sub>COOC(CH<sub>3</sub>)<sub>3</sub>), 51.8-49.8 (macrocycle), 44.6-43.8 (-NCH<sub>2</sub> pip), 28.0 (-C(CH<sub>3</sub>)<sub>3</sub>), 26.3 (-NCH<sub>2</sub>CH<sub>2</sub>-pip), 25.4 (-NCH<sub>2</sub>CH<sub>2</sub>-pip), 24.2 (-NCH<sub>2</sub>CH<sub>2</sub>CH<sub>2</sub>-pip). ESI-MS (m/z): found 670.81 (M+H<sup>+</sup>) (calc for C<sub>36</sub>H<sub>62</sub>N<sub>5</sub>O<sub>8</sub>:670.91).

### I.6. Synthesis of 2,2',2''-(10-(3-amino-2-hydroxy-3-oxopropyl)-1,4,7,10-tetraazacyclododecane-1,4,7-triyl) triacetic acid (**HPADO3A**, **L1**)

**L1**(*t*Bu)<sub>3</sub> (86 mg, 0.14 mmol) was dissolved in DCM: TFA (1:1/ v:v) (4 ml) and stirred at room temperature for 16 hours. After the evaporation of the solvent in vacuo, the mixture was purified in semi-preparative HPLC-MS with the method reported in paragraph 1.1 (Semi-preparative HPLC-MS (Method 2): t<sub>r</sub>= 7.1 min.) After HPLC-MS purification, the ligand **L1** was dissolved in HCl 1M (1 ml) and evaporated in vacuo. This operation was repeated twice

and finally the aqueous solution was freeze dried to obtain **L1** as HCl salt in 69 % yield (49 mg, 0.098 mmol).  $^1\text{H}$  NMR ( $\text{D}_2\text{O}$ , 500MHz):  $\delta$ = 4.48 (m,  $-\text{NCH}_2\text{CH}(\text{OH})-$ ), 4.10-3.17 (m, macrocycle,  $-\text{NCH}_2\text{COOOH}$ ,  $-\text{NCH}_2\text{CH}(\text{OH})-$ , 22H);  $^{13}\text{C}$  NMR ( $\text{D}_2\text{O}$ , 125MHz):  $\delta$ = 175.7 ( $\text{NCH}_2\text{COOH}$ ), 170.8 ( $(-\text{CH}_2\text{CO}-\text{NH}_2)$ ), 66.9 ( $-\text{NCH}_2\text{CH}(\text{OH})-$ ), 56.8 ( $-\text{NCH}_2\text{CH}(\text{OH})-$ ), 56.3 ( $-\text{NCH}_2\text{COOOH}$ ), 55.9-50.3 (macrocycle). Analytical HPLC-MS (Method A):  $t_r$ = 13.35 min. ESI-MS (m/z): found 434.48 ( $\text{M}+\text{H}^+$ ) (calc for  $\text{C}_{17}\text{H}_{32}\text{N}_5\text{O}_8$ :434.47).

### I.7. Synthesis of 2,2',2''-(10-(2-(benzylamino)-2-oxoethyl)-1,4,7,10-tetraazacyclododecane-1,4,7-triyl)triacetic acid (BzHPADO3A, L2)

**L2**(*t*Bu)<sub>3</sub> (36 mg, 0.053 mmol) was dissolved in DCM: TFA (1:1/ v:v) (4 ml) and left stirred at rt, for 16 hours After the evaporation of the solvent in vacuo, the mixture was purified in semi-preparative HPLC-MS with the method reported in paragraph 1.1. (Semi-preparative HPLC-MS, Method 2,  $t_r$ = 10.58 min.). After HPLC-MS purification, the ligand **L2** was dissolved in HCl 1M (1 ml) and evaporated in vacuo. This operation was repeated twice and finally the aqueous solution was freeze dried to obtain **L2** as HCl salt in 73% yield (23 mg, 0.039 mmol).  $^1\text{H}$  NMR ( $\text{D}_2\text{O}$ , 500MHz):  $\delta$ = 7.42-7.34 (m, 5H,  $-\text{NCH}_2\text{Ar}$ ), 4.8 (bs,  $-\text{NCH}_2\text{Ar}$ , underneath water peak), 4.44 (m, 1H,  $-\text{NCH}_2\text{CH}(\text{OH})-$ ), 3.65-3.06 (m, macrocycle,  $-\text{NCH}_2\text{COOOH}$ , 22H),  $^{13}\text{C}$  NMR ( $\text{D}_2\text{O}$ , 125MHz):  $\delta$ = 172.9 ( $-\text{NCH}_2\text{COOH}$ ), 169.5 ( $-\text{CH}_2\text{CONH}-$ ), 137.7 (Ph-*ipso*), 128.9 (Ph-*meta*), 127.9 (Ph-*para*), 127.4 (Ph-*ortho*), 66.3 ( $-\text{NCH}_2\text{CH}(\text{OH})-$ ), 55.3 ( $-\text{NCH}_2\text{CH}(\text{OH})-$ ), 54.5 ( $-\text{NCH}_2\text{COOH}$ ), 51.3-48.5 (macrocycle), 43.1 ( $-\text{CH}_2\text{Ph}$ ). Analytical HPLC-MS (Method A):  $t_r$ = 9.92 min. ESI-MS (m/z): found 524.59 ( $\text{M}+\text{H}^+$ ) (calc for  $\text{C}_{24}\text{H}_{38}\text{N}_5\text{O}_8$ : 524.60).

### I.8. Synthesis of 2,2',2''-(10-(2-oxo-2-(piperidin-1-yl)ethyl)-1,4,7,10-tetraazacyclododecane-1,4,7-triyl)triacetic acid (PipHPADO3A, L3)

**L3**(*t*Bu)<sub>3</sub> (54 mg, 0.081 mmol) was dissolved in DCM: TFA (1:1/ v:v) (4 ml) and stirred at rt for 16 hours. After the evaporation of the solvent in vacuo, the mixture was purified in semi-preparative HPLC-MS with the method reported in paragraph 1.1. (Semi-preparative HPLC-MS (Method 2):  $t_r$ = 11.43 min.) After HPLC-MS purification, the ligand **L3** was dissolved in HCl 1M (1 ml) and evaporated in vacuo. This operation was repeated twice and finally the aqueous solution was freeze dried to obtain **L3** as HCl salt in 65% yield (30 mg, 0.052 mmol).  $^1\text{H}$  NMR ( $\text{D}_2\text{O}$ , 500MHz):  $\delta$ = 4.61 (m, 1H,  $-\text{NCH}_2\text{CH}(\text{OH})-$ ), 3.64-3.03 (m, macrocycle,  $-\text{NCH}_2\text{COOH}$ ,  $-\text{NCH}_2(\text{CH}_2)_3-$ ,  $-\text{NCH}_2\text{CH}(\text{OH})-$ , 28H), 1.67-1.45 (m, 6H,  $-\text{NCH}_2(\text{CH}_2)_3-$ ).  $^{13}\text{C}$  NMR ( $\text{D}_2\text{O}$ , 125MHz):  $\delta$ = 177.4 ( $-\text{NCH}_2\text{COOH}$ ), 173.4 ( $-\text{CH}_2\text{CONH}_2$ ), 66.8( $-\text{NCH}_2\text{CH}(\text{OH})-$ ), 54.8 ( $-\text{NCH}_2\text{CH}(\text{OH})-$ ), 53.4 ( $-\text{NCH}_2\text{COOH}$ ), 50.9-46.8 (macrocycle), 44.3-44.0 ( $-\text{NCH}_2\text{-pip}$ ), 26.0-25.1 ( $-\text{NCH}_2\text{CH}_2\text{-pip}$ ), 23.6 ( $-\text{NCH}_2\text{CH}_2\text{CH}_2\text{-pip}$ ). Analytical HPLC-MS (Method A):  $t_r$ = 12.43 min; ESI-MS (m/z): found 502.61 ( $\text{M}+\text{H}^+$ ) (calc for  $\text{C}_{22}\text{H}_{40}\text{N}_5\text{O}_8$ : 502.59).

### I.9. Preparation of Ln<sup>III</sup>-complexes

HPADO3A-ligands (**L1**, 20 mg, 0.046 mmol; **L2**, 26 mg, 0.053 mmol, **L3**, 36 mg, 0.08 mmol) were dissolved in H<sub>2</sub>O (1 mL) and a slight stoichiometric excess (5-10%) of LnCl<sub>3</sub> dissolved in H<sub>2</sub>O (0.2 mL) was added, maintaining the pH  $\approx$  7 by small addition of NaOH 0.1 M solution. Then the solution was stirred for 16 hours at room temperature. Subsequently, the pH was raised to 9.5 to allow precipitation of excess Ln(OH)<sub>3</sub> that was filtered through 0.2  $\mu\text{m}$  filters. Finally, the pH was brought to 7 and the solution was lyophilized to obtain the final complexes. This procedure ensures the absence of excess ligand or free metal ion in the final solution. In fact, the xylenol orange indicator verified the absence of free Ln(III).

**Gd(HPADO3A)**: analytical HPLC-MS (Method 1):  $t_r$ = 7.13 min. ESI-HRMS (m/z): found 611.1070 [ $\text{M}+\text{Na}$ ]<sup>+</sup>, (calc for  $\text{C}_{17}\text{H}_{28}\text{GdN}_5\text{NaO}_8$ : 611.1076).

**Gd(Bz-HPADO3A)**: analytical HPLC-MS (Method 1):  $t_r$ = 11.73 min. ESI-HRMS (m/z): found 701.1541  $[M+Na]^+$ , (calc for  $C_{24}H_{34}GdN_5NaO_8$ : 701.1546).

**Gd(Pip-HPADO3A)**: analytical HPLC-MS (Method 1):  $t_r$ = 12.71 min. ESI-HRMS (m/z): found 679.1696  $[M+Na]^+$ , (calc for  $C_{22}H_{36}GdN_5NaO_8$ : 679.1702).

**Eu(HPADO3A)**: ESI-MS (m/z): found 605.2  $[M+Na]^+$ , (calc for  $C_{17}H_{28}EuN_5NaO_8$ : 605.4).

**Eu(Bz-HPADO3A)**: ESI-MS (m/z): found 795.3  $[M+Na]^+$ , (calc for  $C_{24}H_{34}EuN_5NaO_8$ : 695.5).

**Eu(Pip-HPADO3A)**: ESI-MS (m/z): found 673.2  $[M+Na]^+$ , (calc for  $C_{22}H_{36}EuN_5NaO_8$ : 673.5).

## II. Protonation and complexation equilibria of HPADO3A ligands:

### II.1 Experimental

*Materials*: The chemicals used for the experiments were of the highest analytical grade. The concentration of the  $CaCl_2$ ,  $ZnCl_2$ ,  $CuCl_2$  and  $GdCl_3$  solutions were determined by complexometric titration with standardized  $Na_2H_2EDTA$  and *xylene orange* ( $ZnCl_2$ , and  $LnCl_3$ ), *murexid* ( $CuCl_2$ ) and *Patton & Reeder* ( $CaCl_2$ ) as indicators. The concentration of the  $H_3HPADO3A$  was determined by pH-potentiometric titration in the presence and absence of a large (40-fold) excess of  $CaCl_2$ . The pH-potentiometric titrations were made with standardized 0.2 M NaOH.

*Equilibrium measurements*: The stability and protonation constants of  $Ca^{2+}$ ,  $Zn^{2+}$  and  $Cu^{2+}$  complexes formed with HPADO3A ligand were determined by pH-potentiometric titration. The metal-to-ligand concentration ratio was 1:1 (the concentration of the ligand was generally 0.002 M). The protonation constants of the Gd(HPADO3A), Gd(Bz-HPADO3A) and Gd(Pip-HPADO3A) complexes were determined using pH-potentiometry by titrating the pre-prepared complexes from pH=4.0 to pH=12 with 0.2 M NaOH. The stability constants of the Gd(HPADO3A) complex was determined by the “out-of-cell” technique because of the slow formation reaction. The pH range of the complexation equilibria and the time needed to reach the equilibria were determined by relaxometry for the formation of Gd(HPADO3A). Eight  $Gd^{3+}$  - HPADO3A samples were prepared, which had pH values in the range of 2.5 – 4.0 at equilibrium ( $[Gd^{3+}]=[L]=0.002$  M). The samples were kept at 25°C for 6 weeks to reach equilibrium. For the calculation of the stability constants of the Gd(HPADO3A) complex, besides the protonation constants of ligands, the stability constants of the di-protonated \*Gd( $H_2HPADO3A$ ) out-of-cage complexes (considered as intermediates) was also used as fixed values, which were calculated from the pH-potentiometric titration curve of the  $Gd^{3+}$  - HPADO3A system obtained in the pH range of 1.7 – 4.0.

For the pH measurements and titrations, *Metrohm 888 Titrando* titration workstation *Metrohm-6.0234.110* combined electrode was used. Equilibrium measurements were carried out at a constant ionic strength (0.15 M NaCl) in 6 ml samples at 25 °C. The solutions were stirred, and  $N_2$  was bubbled through them. The titrations were made in the pH range of 1.7-12.0. KH-phthalate (pH=4.005) and borax (pH=9.177) buffers were used to calibrate the pH meter, For the calculation of  $[H^+]$  from the measured pH values, the method proposed by *Irving et al.* was used as follows.<sup>1</sup> A 0.01M HCl solution was titrated with standardized NaOH solution at 0.15 M NaCl ionic strength. The differences ( $A$ ) between the measured ( $pH_{read}$ ) and calculated pH ( $-\log[H^+]$ ) values were used to obtain the equilibrium  $H^+$  concentration from the pH values measured in the titration experiments ( $A=0.024$ ). For the equilibrium calculations, the stoichiometric water ionic product ( $pK_w$ ) was also needed to calculate  $[OH^-]$  values under basic conditions. The  $V_{NaOH} - pH_{read}$  data pairs of the HCl – NaOH titration obtained in the pH range 10.5 – 12.0 were used to calculate the  $pK_w$  value ( $pK_w=13.85$ ).

The stability constants of the Cu(HPADO3A) complex were determined by spectrophotometry studying the Cu<sup>2+</sup> - HPADO3A systems at the absorption band of Cu<sup>2+</sup> complexes at [H<sup>+</sup>] = 0.01 – 1.0 M in the wavelength range of 400-800 nm. The concentrations of Cu<sup>2+</sup>, HPADO3A were 0.002 M. The H<sup>+</sup> concentration in the samples was adjusted with the addition of calculated amounts of 3 M HCl (I=[Na<sup>+</sup>]+[H<sup>+</sup>]=0.15, [H<sup>+</sup>]≤0.15 M). The samples were kept at 25°C for a week. The absorbance values of the samples were determined at 11 wavelengths (575, 595, 615, 635, 655, 675, 695, 715, 735, 755 and 775 nm). For the calculations of the stability and protonation constants of the Cu(HPADO3A), the molar absorptivities of CuCl<sub>2</sub>, Cu(HPADO3A), Cu(HHPADO3A) and Cu(H<sub>2</sub>HPADO3A) were determined by recording the spectra of 1.0×10<sup>-3</sup>, 1.5×10<sup>-3</sup>, 2.0×10<sup>-3</sup> and 2.5×10<sup>-3</sup> M solutions of CuCl<sub>2</sub> and Cu(HPADO3A) in the pH range of 1.7 – 7.5. The pH was adjusted by stepwise addition of concentrated NaOH or HCl solutions. The spectrophotometric measurements were made with the use of *PerkinElmer Lambda 365 UV-Vis* spectrophotometer at 25 °C, using 1.0 cm cells. The protonation and stability constants were calculated with the PSEQUAD program.<sup>2</sup>

## II.2. Acid-base properties of H<sub>3</sub>HPADO3A ligands.

The protonation constants, defined by Equation (1), were determined by pH-potentiometry.

$$K_i^H = \frac{[H_iL]}{[H_{i-1}L][H^+]} \quad (1)$$

where i=1, 2...6. The logK<sub>i</sub><sup>H</sup> values obtained by pH-potentiometry are listed and compared with those of H<sub>4</sub>DOTA, H<sub>3</sub>HPADO3A, H<sub>3</sub>BT-DO3A ligands in Table S1. Standard deviations (3σ) are shown in parentheses. The protonation sequence of the macrocyclic DOTA-like ligands has been fully characterized with both spectroscopic and potentiometric methods.<sup>3</sup> By taking into account these data, we may safely assume that the first and second protonation of HPADO3A take place at two opposite ring nitrogen atoms, whereas the third protonation process occurs at the carboxylate groups of the acetic arms attached to the non-protonated ring nitrogen atoms of HPADO3A, due to the greater charge separation and lower electrostatic repulsion between the protonated donor atoms. Further protonation of HPADO3A occurs at the non-protonated carboxylate pendant arms.

Comparison of the protonation constants of HPADO3A with those of DOTA, HPADO3A and BT-DO3A indicates that the logK<sub>1</sub><sup>H</sup> value of HPADO3A is somewhat lower, whereas its logK<sub>2</sub><sup>H</sup> and logK<sub>3</sub><sup>H</sup> values are comparable with those of the related logK<sub>i</sub><sup>H</sup> values of the HPADO3A and BT-DO3A ligands. The electron withdrawing effect of the hydroxypropionamide function might explain the lower first protonation constant of HPADO3A.

**Table S1.** Protonation constants of HPADO3A, HPDO3A, DOTA and BT-DO3A at 25°C

	<b>HPADO3A</b>	<b>DOTA<sup>a</sup></b>	<b>HPDO3A<sup>c</sup></b>	<b>BT-DO3A<sup>d</sup></b>
<b>I</b>	0.15 M NaCl	0.1 M KCl	0.1 M Me <sub>4</sub> NCl	0.1 M NaCl
logK <sub>1</sub> <sup>H</sup>	8.96 (1)	11.14	11.96	9.46
logK <sub>2</sub> <sup>H</sup>	9.07 (1)	9.69	9.43	9.36
logK <sub>3</sub> <sup>H</sup>	4.22 (1)	4.85	4.30	4.17
logK <sub>4</sub> <sup>H</sup>	2.64 (1)	3.95	3.26	3.02
logK <sub>5</sub> <sup>H</sup>	1.25 (1)	–	–	–
<b>CaL</b>	<b>12.13 (4)</b>	<b>16.37</b>	<b>14.83</b>	<b>12.1</b>
CaHL	4.67 (5)	3.60	–	–
Ca(L)H <sub>1</sub>	11.50 (6)	–	–	–
<b>ZnL</b>	<b>17.18 (3)</b>	<b>18.7</b>	<b>19.37</b>	<b>17.0</b>
ZnHL	3.67 (2)	5.33	3.7	4.3
ZnH <sub>2</sub> L	2.87 (2)	3.96	–	–
Zn(L)H <sub>1</sub>	10.79 (5)	10.62	–	–
<b>CuL</b>	<b>21.53 (2)</b>	<b>22.72</b>	<b>22.84</b>	<b>19.1</b>
CuHL	4.00 (3)	4.45	3.72	3.8
CuH <sub>2</sub> L	1.24 (3)	3.92	2.3	2.4
Cu(L)H <sub>1</sub>	10.55 (2)	–	–	–
<b>GdL</b>	<b>18.41 (2)</b>	<b>24.7<sup>b</sup></b>	<b>23.8</b>	<b>18.7</b>
*GdH <sub>2</sub> L	5.72 (1)	6.07 (1)	5.10 (1)	4.53 (5)
<b>Gd(L)H<sub>1</sub></b>	<b>6.73 (4)</b>	–	<b>11.36<sup>d</sup></b>	<b>9.48<sup>d</sup></b>

<sup>a</sup> Ref. [4]; 0.1 M KCl, 25°C; <sup>b</sup>Ref. [5], 0.1 M NaCl, 25°C; <sup>c</sup> Ref. [6], 0.1 M Me<sub>4</sub>NCl, 25 °C; <sup>d</sup> Ref. [7], 0.1 M NaCl, 25°C; \* stability constants of the protonated \*Gd(H<sub>2</sub>L) out-of-cage complex (intermediate) \*K<sub>Gd(HiL)</sub>=[Gd(H<sub>2</sub>L)]/[Gd<sup>3+</sup>][H<sub>2</sub>L], 0.15 M NaCl, 25°C; Gd(Bz-HPADO3A): logK<sub>Gd(L)H-1</sub>=7.08 (5); Gd(Pip-HPADO3A): logK<sub>Gd(L)H-1</sub>=6.82 (2) , 0.15 M NaCl, 25°C

### II.3. Complexation features of HPADO3A ligands

The stability and protonation constants of Ca<sup>2+</sup>, Zn<sup>2+</sup>, Cu<sup>2+</sup> and Gd<sup>3+</sup> complexes of HPADO3A, defined by Eqs. (2) and (3), were investigated by pH-potentiometry and spectrophotometry at 25 °C in 0.15 M NaCl solution.

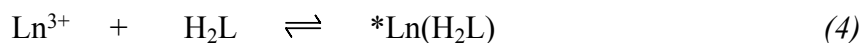
$$K_{ML} = \frac{[ML]}{[M][L]} \quad (2)$$

$$K_{MH_iL} = \frac{[MH_iL]}{[MH_{i-1}L][H^+]} \quad (3)$$

where i=0, 1, 2, 3. The K<sub>ML</sub> and K<sub>MHiL</sub> values characterizing the formation of HPADO3A complexes of Ca<sup>2+</sup>, Zn<sup>2+</sup>, Cu<sup>2+</sup> and Gd<sup>2+</sup> have been calculated from the pH-potentiometric titration data obtained at 1:1 metal to ligand concentration ratios. In calculating the equilibrium constants, the best fitting of the mL NaOH – pH data has been obtained by

assuming the formation of ML, MHL, MH<sub>2</sub>L and MLH<sub>1</sub> complexes. The formation of the deprotonated [M(HPADO3A)H<sub>1</sub>]<sup>n-</sup> complexes takes place at pH>8.5, as indicated by the base consumption in the titration curves (M=Ca<sup>2+</sup>, Zn<sup>2+</sup> and Cu<sup>2+</sup>, n=2). This deprotonation occurs on the alcoholic -OH group.

The stability constant of HPADO3A complex formed with Gd<sup>3+</sup> ion has been determined by the “out-of-cell” technique because of the slow complex formation. It is known that the formation of DOTA and DOTA derivative complexes of lanthanides in the pH range 2 – 6 occurs via the formation of a diprotonated “out-of-cage” complex (e.g. \*Ln(H<sub>2</sub>DOTA)). In the “out-of-cage” complex only the carboxylate groups are coordinated to the Ln<sup>3+</sup> ion and two opposite ring nitrogens are protonated.<sup>8</sup> The formation of Ln(DOTA)<sup>-</sup> and their derivative complexes take place by the slow deprotonation of the “out-of-cage” complex (the rate determining step is the loss of the last proton) and by the consequential transformation to the final complex. In the equilibrium systems, the presence of the intermediate, the free Ln<sup>3+</sup> ion and the final Ln(DOTA)<sup>-</sup> complex should also be taken into account.<sup>3</sup> The formation and stability constant of the intermediate is expressed by Eqs (4) and (5).



$$*K_{\text{Ln}(\text{H}_2\text{L})} = \frac{[\text{Ln}(\text{H}_2\text{L})]}{[\text{Ln}^{3+}][\text{H}_2\text{L}]} \quad (5)$$

The “out-of-cage” complexes are formed rapidly, so their stability constants have been determined by direct pH-potentiometric titration of Gd<sup>3+</sup> - HPADO3A, Gd<sup>3+</sup> - DOTA, Gd<sup>3+</sup> - HPADO3A and Gd<sup>3+</sup>- BT-DO3A systems at 1:1 metal to ligand concentration ratios in the pH range 1.7 – 4.0. In the “out-of-cell” samples, the measured equilibrium pH values were between 2.0 and 4.0. With the use of the added mL NaOH – pH data, the stability constants of Gd(HPADO3A) complex could be calculated. For the complete characterization of the complexation in Gd<sup>3+</sup>-HPADO3A, Gd<sup>3+</sup>-Bz-HPADO3A and Gd<sup>3+</sup>-Pip-HPADO3A systems, the GdL complexes (which are formed completely at about pH=4.0), have been titrated in the pH range 4.0 – 11.0. During these titrations, base consumption has been observed at about pH>4.5, which indicated the deprotonation of the GdL species. This process is the dissociation of H<sup>+</sup> ion from the alcoholic -OH group of the pendant arm. By taking into account the protonation constant of the HPADO3A ligand, the stability constant of the \*[Gd(H<sub>2</sub>HPADO3A) intermediate and the stability and protonation constant of the Gd(HPADO3A) complex, the species distribution of the Gd<sup>3+</sup> - HPADO3A system has been calculated (Figure S1).

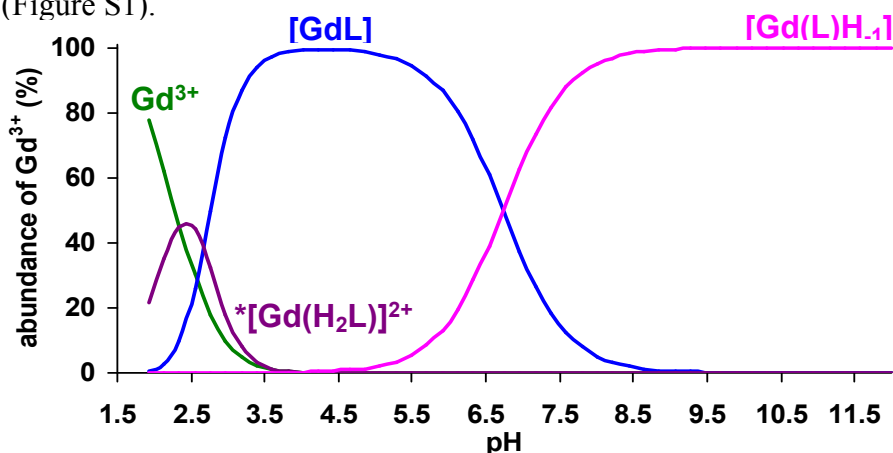


**Figure S1.** Species distribution diagram of the Gd<sup>3+</sup>- HPADO3A system ([Gd<sup>3+</sup>]=[HPADO3A]=1.0 mM, 0,15 M NaCl, 298K)

The stability and protonation constants of Cu(HPADO3A) have been determined by spectrophotometry. The equilibrium reaction (Eq. (6)) has been studied in the  $[H^+]$  range of 0.01 – 1.0 M (the ionic strength were constant  $I=[Na^+]+[H^+]=0.15$  in the samples  $[H^+] \leq 0.15$  M), where the formation of  $Cu^{2+}$ ,  $CuH_2L$  and  $H_xL$  species was assumed ( $x=4$  and 5;  $y=2$  and 3). Some characteristic absorption spectra are shown in Figure S2.

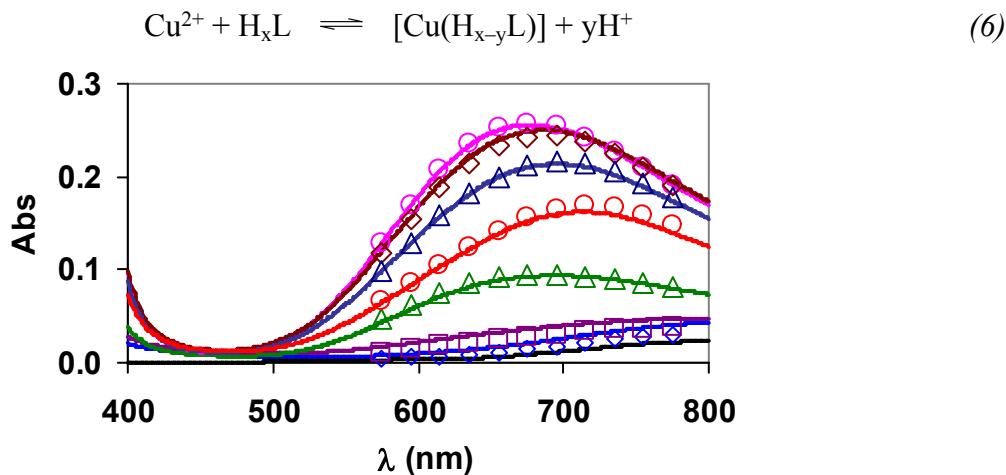


**Figure S2.** Absorbance spectra of  $Cu^{2+}$ -HPADO3A system. The solid lines and the open symbols represent the experimental and the calculated absorbance values, respectively. ( $[Cu^{2+}]=[HPADO3A]=2.0$  mM,  $[H^+] = 1.0$  (\*),  $0.60$  (●),  $0.31$  (□),  $0.10$  (○),  $0.04$  (\*),  $0.025$  (□) and  $0.01$  M (○),  $[Cu^{2+}]=2.0$  mM,  $I=[Na^+]+[H^+]=0.15$ ,  $[H^+] \leq 0.15$  M,  $l=1$  cm,  $25^\circ C$ )

The protonation constants of  $Cu(HPADO3A)^{2-}$  have been determined by pH-potentiometric and spectrophotometric titrations of the complexes in the pH range 1.7 – 12.0, where di-, mono-protonated and deprotonated complexes are present. The species distribution diagram and the maxima of the absorption spectra ( $\lambda_{max}$  values) of  $Cu^{2+}$  - HPADO3A system is shown as functions of pH in Figure S3. The positions of the absorption maxima and the molar absorptivities of  $Cu^{2+}$  and  $Cu(H_xHPADO3A)$  complexes differ considerably (e.g. at 735 nm  $\epsilon_{Cu^{2+}}=10.43$   $cm^{-1}M^{-1}$  and  $\epsilon_{Cu(H_2HPADO3A)}=205.1$   $cm^{-1}M^{-1}$ ). The maximum of the absorption band of  $Cu(H_2HPADO3A)$  is at 665 nm, while that of  $Cu^{2+}$  is at 790 nm. The maximum of the absorption band is shifted from 665 to 730 nm by the deprotonation of  $Cu(H_2HPADO3A)^+$ , whereas the deprotonation of  $Cu(HHPADO3A)$  and the formation of  $Cu(HPADO3A)^-$  species do not affect the absorption maxima (Figure S3). According to the shift of the absorption maxima due to the axial coordination of the different donor atoms,<sup>9</sup> the approximately 60 nm “red” shift observed during the deprotonation of  $Cu(H_2HPADO3A)^+$  species may be explained by the deprotonation and coordination of the ring nitrogen to  $Cu^{2+}$ -ion with the replacement of the  $H_2O$  molecule in axial position.

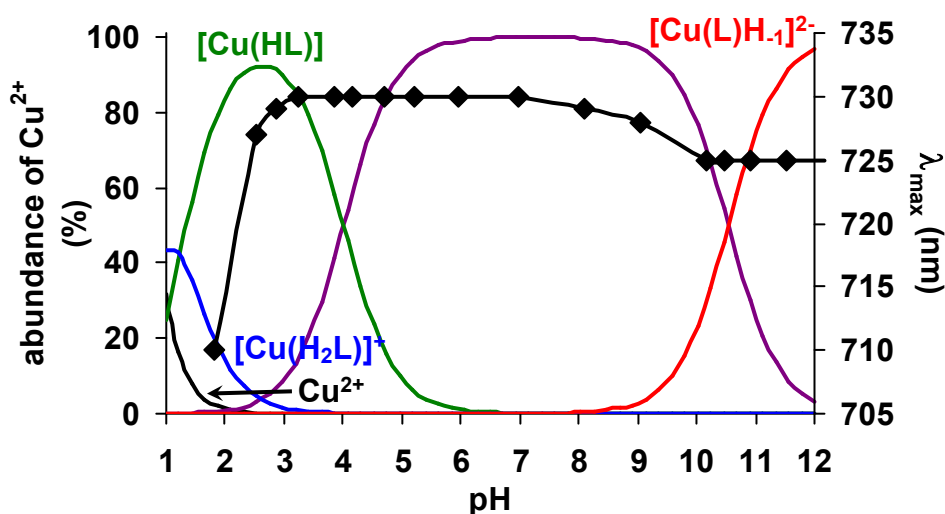


**Figure S3.** Species distribution and the  $\lambda_{\max}$  values (◆) of  $\text{Cu}^{2+}$ - HPADO3A system as a function of pH. ( $[\text{Cu}^{2+}] = [\text{HPADO3A}] = 1.6 \text{ mM}$ ,  $0.15 \text{ M NaCl}$ ,  $25 \text{ }^\circ\text{C}$ )

The structure of  $\text{Cu}(\text{HHPADO3A})$  is presumably very similar to that of  $\text{Cu}(\text{H}_2\text{DOTA})$  complex.<sup>10</sup>  $\text{Cu}(\text{HHPADO3A})$  is characterized by distorted octahedral geometry, in which the  $\text{Cu}^{2+}$ -ion is coordinated by two ring nitrogens and two carboxylate oxygens in equatorial positions and by two ring nitrogens in axial positions, whereas the protonated carboxylate and the alcoholic  $-\text{OH}$  groups do not coordinate the  $\text{Cu}^{2+}$  ion. Further increase of pH does not influence the position of the absorption maxima indicating that the deprotonation of  $\text{Cu}(\text{HHPADO3A})$  takes place at the protonated carboxylate group. In the pH-potentiometric titration of  $\text{Cu}(\text{HPADO3A})^-$ , the base consumption indicates the deprotonation of the  $-\text{OH}$  group at  $\text{pH} > 8.5$ . The formation of  $[\text{Cu}(\text{HPADO3A})\text{H}_{-1}]^{2-}$  results in about 5 nm “blue” shift in the  $\lambda_{\max}$  value (Figure S3). By taking into account the small changes in the  $\lambda_{\max}$  value, we can assume a direct interaction between the  $\text{Cu}^{2+}$ -ion and alcoxide  $-\text{O}^-$  donor atom by substitution of the carboxylate  $-\text{O}^-$  with deprotonated alcoxide  $-\text{O}^-$  donor atom in the equatorial position of  $[\text{Cu}(\text{HPADO3A})\text{H}_{-1}]^{2-}$  species.<sup>9</sup>

The stability constants of the  $\text{Ca}^{\text{II}}$ ,  $\text{Zn}^{\text{II}}$ ,  $\text{Cu}^{\text{II}}$  and  $\text{Gd}^{\text{III}}$  complexes formed with HPADO3A (Table S1) are generally about 1 – 5 orders of magnitude lower than those of the corresponding DOTA and HPADO3A complexes, whereas the  $\log K_{\text{ML}}$  values of HPADO3A and BT-DO3A complexes formed with  $\text{Ca}^{2+}$ ,  $\text{Zn}^{2+}$  and  $\text{Gd}^{3+}$  ions are very similar. For the determination of the stability constants of metal complexes, the protonation constants of the ligands need to be known. It has to be underlined that the protonation constants are determined by using constant ionic background (some salts like KCl, NaCl, etc.) which has to be selected very carefully as its cation can react with the ligand (when the protonation constants are determined) or its counterion may form weak complexes with the metal ion (during the stability constant determination). The  $\log K_1^{\text{H}}$  and  $\log K_{\text{ML}}$  values, published in literature were most frequently determined in 0.1 M KCl or 0.1 M  $\text{Me}_4\text{NCl}$ .<sup>11</sup> The protonation constants of ligands particularly the  $\log K_1^{\text{H}}$  values determined in 0.15 M NaCl solution are generally lower than those obtained in solutions, where the constant ionic strength was controlled by 0.1 M KCl or 0.1 M  $\text{Me}_4\text{NCl}$ . The  $\log K_1^{\text{H}}$  values obtained in NaCl solutions are lower because the interaction between the smaller  $\text{Na}^+$  ion and the fully deprotonated ligands is stronger than that of the larger  $\text{K}^+$  or  $\text{Me}_4\text{N}^+$  ions. The difference is particularly high for macrocyclic ligands which form relatively stable complexes with  $\text{Na}^+$  ( $\log K_{\text{Na}(\text{DOTA})} = 4.38$ ).<sup>12</sup> The stability constant of  $\text{Gd}(\text{HPADO3A})$  (Table S1) is significantly lower than that of  $\text{Gd}(\text{HPADO3A})$

determined by *Kumar et al.* in 0.1 M Me<sub>4</sub>NCl ( $\log K_{\text{GdL}}=23.8$ )<sup>6</sup> (due to the significantly higher  $\log K_{\text{I}^{\text{H}}}$  value of HPDO3A determined in 0.1 M Me<sub>4</sub>NCl solution. However, the  $\log K_{\text{GdL}}$  values of Gd(HPADO3A) and Gd(BT-DO3A) obtained under similar condition are comparable because the coordinated -OH group of the ligands may have similar role in the Gd<sup>3+</sup> - ligand interaction.

The stability constants of the Ca<sup>II</sup>- and Zn<sup>II</sup>-complexes formed with HPADO3A and BT-DO3A ligands are very similar because the two octadentate ligands are probably coordinated to the Ca<sup>2+</sup> and Zn<sup>2+</sup> ions by the same donor atoms. Moreover, the similar stability of Zn(HPADO3A) and Zn(BT-DO3A), and of Ca(HPADO3A) and Ca(BT-DO3A) complexes indicates that the presence of the amide substituent on the pendant arm does not affect the stability of the Zn<sup>II</sup> and Ca<sup>II</sup>-complexes.

The stability constant obtained for the Cu(HPADO3A) ( $\log K_{\text{CuL}}=21.53(2)$ ) is significantly higher than that of Cu(BT-DO3A) ( $\log K_{\text{CuL}}=19.1$ ) published earlier in literature.<sup>7</sup> The possible reason of this large difference is that the formation of the Cu(BT-DO3A) complex was followed by pH-potentiometry at pH>1.7 in the cited paper. Under these conditions, the Cu(H<sub>2</sub>L) species is fully formed and the amount of the free Cu<sup>2+</sup> ion is negligible making the estimation of the  $\log K_{\text{ML}}$  value unreasonable.

The alcoholic -OH group in the pendant arm of the in the Ca<sup>II</sup>, Zn<sup>II</sup> and Cu(HPADO3A) complexes can be deprotonated and the  $\log K_{\text{MLH-1}}$  values (Table S1) are 11.50, 10.79 and 10.55, respectively. The  $\lambda_{\text{max}}$  values in Cu(HPADO3A) UV-vis spectra indicate that the deprotonation of the alcoholic -OH group results in ca. 5 nm “blue” shift in the absorption maxima, which can be interpreted by the direct interaction between the Cu<sup>2+</sup> -ion and alcoxide -O<sup>-</sup> donor atom.<sup>9</sup> However, the deprotonated alcoxide -O<sup>-</sup> donor atom in Ca<sup>II</sup>, Zn<sup>II</sup> and Cu<sup>II</sup> - complexes is weakly coordinated.

On the other hand, the dissociation constants ( $\log K_{\text{Gd(L)H-1}}$ ) of the -OH group in the Gd<sup>III</sup>-complexes formed with HPADO3A, Bz-HPADO3A and Pip-HPADO3A ligands are about 5 – 6 orders of magnitude lower than the those of Ca<sup>II</sup>-, Zn<sup>II</sup>- and Cu(HPADO3A) complexes (Gd(HPADO3A):  $\log K_{\text{Ga(L)H-1}}=6.73(4)$ , Gd(Bz-HPADO3A):  $\log K_{\text{Ga(L)H-1}}=7.08(5)$ , Gd(Pip-HPADO3A):  $\log K_{\text{Ga(L)H-1}}=6.82(2)$ , Table S1). It means that the interaction between the Gd<sup>3+</sup> - ions and the alcoxide -O<sup>-</sup> donor atom is strong, and this binding is responsible for significantly lower dissociation constant of the alcoholic -OH group in Gd(HPADO3A) complexes. By comparing the  $\log K_{\text{Gd(L)H-1}}$  values of Gd(HPADO3A) with those of Gd(HPADO3A) complexes, the lower dissociation constant of the alcoholic -OH group is explained by the substitution of the electron donor -CH<sub>3</sub> with the electron withdrawing amide group to make the alcoholic -OH group more acidic. The  $\log K_{\text{Gd(L)H-1}}$  values of Gd(HPADO3A), Gd(Bz-HPADO3A) and Gd(Pip-HPADO3A) indicate that the substituent of the amide function does not alter the dissociation constant of the alcoholic -OH group.

### III. Kinetic inertness of Gd(HPADO3A) complex

#### III.1. Experimental

The kinetic inertness of the Gd(HPADO3A) was characterized by the rates of the dissociation reactions taking place in 0.01 – 1.0 M HCl solution. The dissociation reactions of the Gd<sup>III</sup>-complex were followed by measuring the longitudinal relaxation time of H<sub>2</sub>O protons ( $T_1$ ) with a Bruker Avance III 400 (9.4 T) spectrometer equipped with BB inverse z gradient probe (5 mm). The temperature of the sample holder was controlled with a thermostated air stream. The longitudinal relaxation time was measured with the “inversion recovery” method (180° -  $\tau$  - 90°) by using 12 different  $\tau$  values. The measurements were performed with 1 mM solution of Gd(HPADO3A) complex. The relaxivity values were given as  $r_1=1/T_{1p} + 1/T_{1w}$

where  $T_{1p}$  and  $T_{1w}$  are the relaxation times of the bulk water protons in the presence and absence of  $Gd^{III}$ -complex. The pseudo-first-order rate constants ( $k_d$ ) were calculated by fitting the relaxation rate ( $r_1=1/T_{1p}$ ) data to Eq. (7).

$$r_t = (r_r - r_v)e^{(-k_d t)} + r_v \quad (7)$$

where  $r_r$ , and  $r_v$  are the relaxivity values of the reactants, the product ( $Gd^{3+}$ :  $r_{1p}= 12.56$  (4)  $mM^{-1}s^{-1}$ , 400 MHz, 25 °C) and  $r_t$  is the measured relaxivity at reaction time  $t$ . The temperature was maintained at 298 K and the ionic strength of the solutions was kept constant at  $[H^+] \leq 0.15$  M,  $[HCl]+[NaCl]=0.15$  M. The calculation of the kinetic parameters were performed by the fitting of the absorbance - time and relaxation rate – time data pairs with the *Micromath Scientist* computer program (version 2.0, Salt Lake City, UT, USA).

### III.2. Dissociation kinetics of Gd(HPADO3A)

The dissociation reactions of Gd(HPADO3A) have been studied by  $^1H$ -NMR relaxometry in 0.01 – 1.0 M HCl solution to guarantee the pseudo-first-order kinetic condition. The  $r_1^{obs}$  values as a function of time for the dissociation reactions of Gd(HPADO3A) are shown in Figure S4.

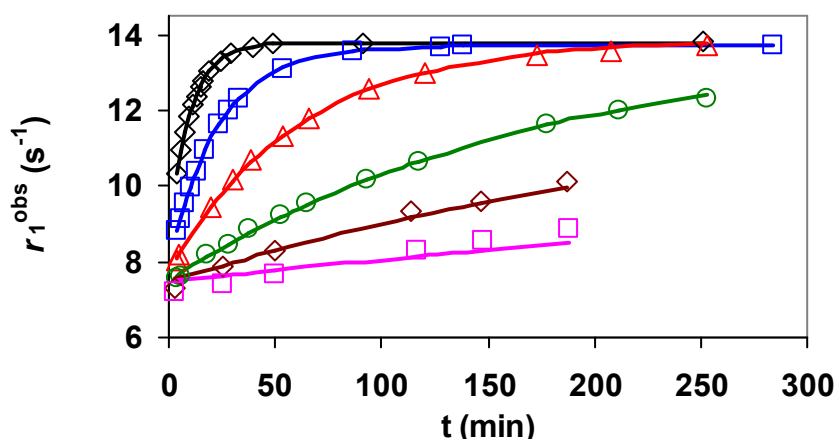


**Figure S4.**  $r_1^{obs}$  values of Gd-HPADO3A complex as a function of time in the presence of 1.00 (\*), 0.40 (●), 0.16 (□), 0.06 (▲), 0.025 (\*) and 0.010 M (◐) HCl, ( $[Gd(HPADO3A)]=1.0$  mM,  $[H^+] \leq 0.15$  M  $\rightarrow$   $[Na^+]+[H^+]=0.15$  M, 25°C)

In the presence of HCl excess, the decomplexation of Gd(HPADO3A) can be treated as a pseudo-first-order process and the reaction rate can be expressed by Eq. (8), where  $k_d$  is a pseudo-first-order rate constant,  $[GdL]_t$  and  $[GdL]_{tot}$  are the concentrations of the GdL species at time  $t$  and the total concentration of the complex, respectively.

$$-\frac{d[GdL]_t}{dt} = k_d [GdL]_{tot} \quad (8)$$

The rates of the transmetallation reactions have been studied at different concentrations of the HCl ( $[HCl]=0.01 - 1.0$  M, 25°C). The  $k_d$  values as a function of  $[H^+]$  are shown in Figure S5.

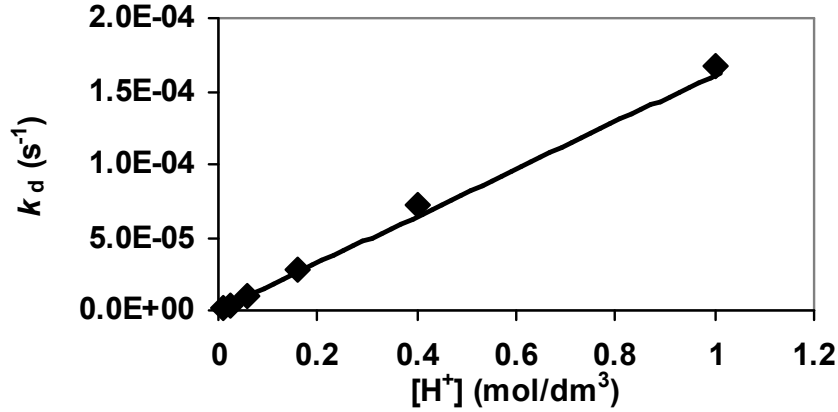
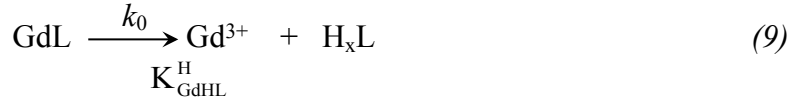


**Figure S5.** Pseudo-first-order rate constant ( $k_d$ ) characterizes the dissociation of Gd(HPADO3A) as a function of  $[H^+]$  ( $[Gd(HPADO3A)]=1.0$  mM,  $[H^+] \leq 0.15$  M  $\rightarrow [Na^+] + [H^+] = 0.15$  M, 25°C).

The obtained  $k_d$  pseudo-first order rate constants are directly proportional to the concentration of  $H^+$ . The increase in the  $k_d$  values with increasing concentration of  $H^+$  can be interpreted in terms of the proton assisted dissociation of Gd(HPADO3A). The dependence of  $k_d$  on  $[H^+]$  can be expressed as a first-order function of  $[H^+]$  which indicates that the exchange can take place by proton-independent (Eq. (9)) and proton assisted (Eq. (11)) pathways. The proton assisted dissociation of Gd(HPADO3A) might be explained by the equilibrium formation of a protonated Gd(HHPADO3A) intermediate (Eq. (10)), which dissociate spontaneously (Eq. (12)).



$$K_{GdHL}^H = \frac{[Gd(HL)]}{[GdL][H^+]}$$



$k_0$  and  $k_{GdHL}$  are the rate constants which characterize the dissociation of Gd(HPADO3A) via spontaneous and proton-assisted reaction pathways, respectively. The  $K_{GdHL}^H$  is the protonation constant of Gd(HPADO3A) complex. By considering all the possible pathways and the rate of dissociation of Gd(HPADO3A) (Eq. (8)), the pseudo-first-order rate constant ( $k_d$ ) can be expressed by Eq. (12).

$$-\frac{d[GdL]_t}{dt} = k_0[GdL] + k_{GdHL}[GdHL] \quad (12)$$

By taking into account the total concentration of the complex ( $[GdL]_{tot} = [GdL] + [Gd(HL)]$ ), the protonation constants of the Gd(HPADO3A) ( $K_{GdHL}^H$ , Eq. (10)) and Eq. (12), the pseudo-first-order rate constant ( $k_d$ ) can be expressed as follows:

$$k_d = \frac{k_0 + k_1[H^+]}{1 + K_{GdHL}^H[H^+]} \quad (13)$$

where  $k_0$ , and  $k_1 = k_{\text{GdHL}} \times K_{\text{GdHL}}^{\text{H}}$  are the rate constants characterizing the spontaneous and proton-assisted dissociation of Gd(HPADO3A). The protonation constant ( $K_{\text{GdHL}}^{\text{H}}$ ) of Gd(DOTA)-like complexes are relatively small (Gd(DOTA):  $K_{\text{GdHL}}^{\text{H}} = 14$ ).<sup>[8a]</sup> However, the protonation process could not be detected in the pH-potentiometric studies of Gd(HPADO3A) complex. By taking into account the very low protonation constant of Gd(HPADO3A) ( $K_{\text{GdHL}}^{\text{H}} \ll 10$ ), the denominator of Eq. (13) ( $1 \gg K_{\text{GdHL}}^{\text{H}} [\text{H}^+]$ ) can be neglected, so Eq. (13) can be simplified in the form of Eq. (14). The  $k_0$  and  $k_1$  values have been calculated by fitting of the kinetic data (Figure S5) to Eq. (14).

$$k_d = k_0 + k_1[\text{H}^+] \quad (14)$$

#### IV. Effect of $\text{NH}_4\text{Cl}$ for the proton exchange processes of Gd(HPADO3A), Gd(Bz-HPADO3A) and Gd(Pip-HPADO3A) complexes

In order to get insight into the mechanism of the acid-base catalyzed proton exchange processes of Gd(HPADO3A) derivatives, the relaxivity values of Gd(HPADO3A), Gd(Bz-HPADO3A), Gd(Pip-HPADO3A) were measured at pH=6.0, 298 K and 20 MHz in the absence and in the presence of  $\text{NH}_4\text{Cl}$  as general acid (Figure S6).

As shown in Figure S6,  $\text{NH}_4\text{Cl}$  yields the increase of the relaxivity values of Gd(HPADO3A), Gd(Bz-HPADO3A) and Gd(Pip-HPADO3A) at pH=6.0. These relaxation effects are due to the enhancement of the proton exchange of the Gd(HPADO3A), Gd(Bz-HPADO3A) and Gd(Pip-HPADO3A) with the bulk. By taking into account the protonation constant of  $\text{NH}_3$  ( $\log K^{\text{H}} = 9.36$ , 0.1 M  $\text{NaNO}_3$ , 25°C),<sup>13</sup> the  $\text{NH}_4^+$  cation is dominant at pH=6.0 and 25°C in 0.15 M NaCl solution.

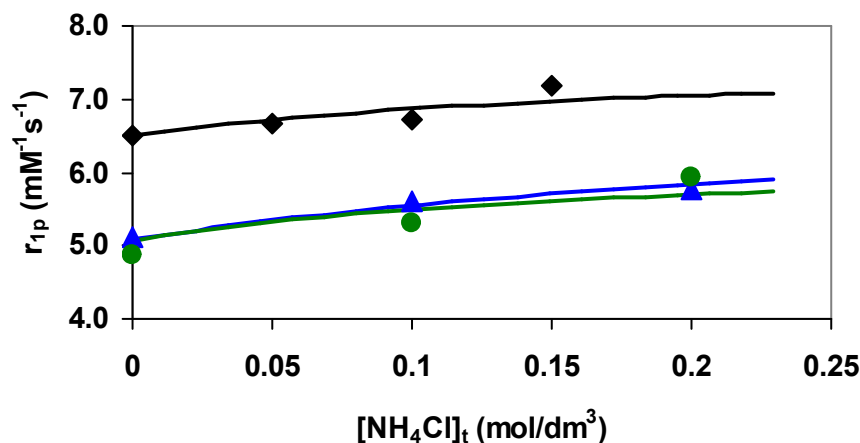
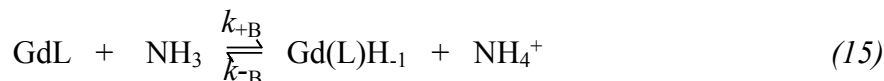


**Figure S6.** The relaxivity of Gd(HPADO3A) (⊕), Gd(Bz-HPADO3A) (⊠) and Gd(Pip-HPADO3A) (⊗) as a function of  $[\text{NH}_4\text{Cl}]$ . ( $[\text{GdL}] = 1.0$  mM, pH=6.0, 20 MHz, 0.15 M NaCl, 298 K).

The  $[\text{NH}_4\text{Cl}]$  dependent relaxation enhancements in Figure S6 can readily be interpreted by considering general base catalyzed proton exchange reactions. Since the noted relaxation enhancement of Gd(HPADO3A), Gd(Bz-HPADO3A) and Gd(Pip-HPADO3A) at pH=6.0 are essentially identical ( $\Delta r_1 = 0.8$  mM<sup>-1</sup>s<sup>-1</sup>, Figure S6), it is reasonable to assume that only the -OH proton of the Gd(HPADO3A) derivatives takes place in the  $\text{NH}_3/\text{NH}_4^+$  assisted exchange process with the bulk (Eq. (15)).



where  $v_+ = k_{+B}[\text{NH}_3]$  ;  $v_- = k_{-B}[\text{NH}_4^+]$ ,  $k_{+B}$  and  $k_{-B}$  are the rate and rate constants of the forward and backward reactions, respectively. The lifetime of the alcoholic –OH proton is  $\tau_p = (k_{+B}[\text{NH}_3])^{-1}$ . By taking into account the  $\text{H}^+$  and  $\text{NH}_3$  assisted exchange processes of the labile protons in Gd(HPA-DO3A) derivatives with the bulk water ( $k_H$  and  $k_{+B}$ ), the protonation/deprotonation of the –OH group ( $K_{\text{Gd(L)H-1}}$ ) and the different  $r_1^{\text{is}}$  and  $r_1^{\text{os}}$  values of the protonated GdL and the deprotonated Gd(L)H<sub>-1</sub> species ( $^{\text{GdL}}r_1^{\text{is+os}}$  and  $^{\text{Gd(L)H-1}}r_1^{\text{is+os}}$ ), the relaxivity value in Figure S6 can be expressed by Eq. (16) :

$$r_{1p} = \frac{1}{1 + K_{\text{Gd(L)H-1}}[\text{H}^+]}\left[ K_{\text{Gd(L)H-1}}[\text{H}^+]^{\text{GdL}} r_1^{\text{is+os}} + ^{\text{Gd(L)H-1}}r_1^{\text{is+os}} + \frac{cK_{\text{Gd(L)H-1}}[\text{H}^+]}{111.1} \left( \frac{N}{T_{1p}^{\text{H}} + (k_{\text{H}}[\text{H}^+])^{-1}} + \frac{1}{T_{1p}^{\text{H}} + (k_{+B}[\text{NH}_3])^{-1}} \right) \right] \quad (16)$$

The experimental data were fitted to Eq. (16) using a non-linear least squares algorithm. The equilibrium concentrations of the acid and basic forms of the  $\text{NH}_3$  were calculated by using the corresponding protonation constants of  $\text{NH}_3$  ( $\log K^{\text{H}}=9.36$ ).<sup>13</sup> Rate constant  $k_H$  and the longitudinal relaxation time  $T_{1p}^{\text{H}}$  of the alcoholic –OH and amide –CONH<sub>n</sub>– protons of Gd(HPA-DO3A) derivatives were fixed at the value obtained in the absence of  $\text{NH}_4\text{Cl}$ . The calculate rate constants,  $k_{+B}$  are essentially equal (Gd(HPADO3A):  $k_{+B}=(1.8\pm 0.3)\times 10^9 \text{ M}^{-1}\text{s}^{-1}$ , Gd(Bz-HPADO3A):  $k_{+B}=(2.5\pm 0.5)\times 10^9 \text{ M}^{-1}\text{s}^{-1}$  and Gd(-Pip-HPADO3A):  $k_{+B}=(2.3\pm 0.8)\times 10^9 \text{ M}^{-1}\text{s}^{-1}$ ) and somewhat lower than the  $k_{\text{OH}}$  value characterizing the OH<sup>-</sup> ion assisted diffusion controlled proton exchange process of the –OH proton in Gd(HP-DO3A) ( $k_{\text{OH}}=1.0\times 10^{10} \text{ M}^{-1}\text{s}^{-1}$ ).<sup>14</sup>

## V. Relaxometric study

### V.1. Experimental

The observed water protons longitudinal relaxation rate ( $R_1^{\text{obs}}$ ) values were measured on a Stellar SpinMaster Spectrometer (Stellar Snc, Mede (PV), Italy) operating at 20 MHz by using the standard inversion recovery pulse sequence with 4 scans for each acquired data point. A precise control of the temperature was operated during the measurements by means of a Stellar VTC-91 airflow heater equipped with a calibrated copper constantan thermocouple (uncertainty of  $\pm 0.1^\circ\text{C}$ ). Furthermore, the real temperature inside the probe head was additionally monitored by a Fluke 52 k/j digital thermometer (Fluke, Zürich, Switzerland). The gadolinium concentration was determined by measuring the bulk magnetic susceptibility shifts of the *t*-BuOH <sup>1</sup>H NMR signal.<sup>15</sup> The proton  $1/T_1$  NMRD profiles of aqueous solutions ( $[\text{GdL}] = 1.0 \text{ mM}$ ) of Gd(HPADO3A) complexes were measured with a fast-field-cycling Stellar SmartTracer relaxometer over a continuum of magnetic field strengths from 0.00024 to 0.25 T (corresponding to 0.01–10 MHz proton Larmor frequencies). The relaxometer was operated under computer control with an absolute uncertainty in  $1/T_1$  of  $\pm 1 \%$ . For the samples at pH 4.2, additional data points in the range 15–70 MHz were obtained with a Bruker WP80 NMR electromagnet adapted to variable-field measurements (15–80 MHz proton Larmor frequency) and a Stellar relaxometer. For the samples at pH 7.4, the additional data points in the range 20–120 MHz were obtained with a High Field NMR Relaxometer (Stellar) equipped with a superconducting magnet HS-110 at 3 T.

Variable-temperature <sup>17</sup>O NMR spectroscopy measurements were performed with a Bruker Avance III (11.7 T) spectrometer equipped with a 5 mm probe and standard temperature control units. Aqueous solutions of Gd(HPADO3A) (12.5 mM), Gd(Bz-HPADO3A) (15.8 mM) and Gd(Pip-HPADO3A) (24.8 mM) containing 2.0 % of the <sup>17</sup>O isotope (Cambridge Isotope) was used. The observed transverse relaxation rates were calculated from the signal width at half-height.

## V.2. Relaxometric analysis.

The magnetic field dependence of  $r_1$  (Nuclear Magnetic Relaxation Dispersion (NMRD) profiles) were measured for the three Gd-complexes at pH 4.2 and 7.4 at both 298 and 310 K in the proton Larmor frequency range 0.01 – 70 (or 120) MHz, corresponding to magnetic field strengths varying between  $2.34 \times 10^{-4}$  T and 1.75 (or 3.0) T (Figures S7-S12). The lower values of the relaxivity at 310 K over the entire range of proton Larmor frequencies investigated indicate that  $r_1$  is not limited by the water exchange rate (fast exchange regime) but rather by the rotational motion. The fitting was carried out by using the Solomon-Bloembergen-Morgan<sup>16</sup> and Freed's<sup>17</sup> equations for the inner- (IS) and outer sphere (OS) proton relaxation mechanisms, respectively, and the results are reported in Table S2. Because of the large number of parameters involved in the fitting procedure, some of them are usually fixed to known or reasonable values. The hydration number  $q$  was fixed to 1; the distance between  $\text{Gd}^{3+}$  and the protons of the bound water molecule,  $r$ , was fixed to 3.0 Å; the distance of closest approach,  $a$ , of the outer sphere water molecules to  $\text{Gd}^{3+}$  was set to 4.0 Å and for the relative diffusion coefficient  $D$  standard values of 2.24 and  $3.1 \times 10^{-5} \text{ cm}^2 \text{ s}^{-1}$  (298 and 310 K) were used. The fit was performed using as adjustable parameters  $\tau_R$  and the electronic relaxation parameters  $\Delta^2$  (trace of the squared zero-field splitting, ZFS, tensor) and  $\tau_V$  (correlation time for the modulation of the transient ZFS). The NMRD profiles were analyzed considering also the contribution of second sphere water molecules, *i.e.* water molecules hydrating the complex at a sufficiently short distance from  $\text{Gd}^{3+}$  (ca.  $< 4$  Å) and with a residence time sufficiently long to be affected by the rotation. This contribution is expressed in terms of three additional parameters: the number  $q^{\text{SS}}$  of second sphere water molecules, their mean distance from the metal ion and their rotational correlation time,  $\tau_{R(\text{SS})}$ . The fitting was carried out considering a number of SS water molecules decreasing from the primary to the tertiary amides (from 5 to 3) at a distance of 3.5 Å, an intermediate value between those of water molecules in the inner (3.0 Å) and outer (4.0 Å) solvation shell. Moreover, in the fitting of the NMRD profiles at pH 4.2, a fixed proton exchange contribution to  $r_1$  ( $r_1^{\text{pr}}$ ) at that pH and 298 K was added to the equations (Table S2).

The accurate value of the residence lifetime of coordinated water,  $\tau_M$ , can be obtained through the measurement of the temperature dependence of the  $^{17}\text{O}$  NMR transverse relaxation rate,  $R_2$ , and paramagnetic shift,  $\Delta\omega$ , of the solvent water. The data were measured at 11.7 T in 12.5, 15.8 and 24.8 mM solutions of Gd(HPADO3A), Gd(BzHPADO3A) and Gd(PipHPADO3A), respectively, at pH 7.4. In the case of Gd(HPADO3A) the data were acquired also at pH 4.2. The experimental data are often reported as reduced transverse relaxation rates,  $R_{2r}$ , defined as  $1/T_{2r} = R_{2r} = R_{2p}/pM$ , where  $pM$  is the molar fraction of inner sphere water molecules. The reduced transverse  $^{17}\text{O}$ -relaxation rates and chemical shifts ( $\Delta\omega_r$ ) measured for Gd(HPADO3A) complexes are reported in Figure S8, S10 and S12. In all cases  $1/T_{2r}$  slightly increases with decreasing temperature over the temperature range studied (275-352K), indicating high rate of exchange for the bound water molecule. The data were analyzed in terms of the Swift-Connick theory for  $^{17}\text{O}$  relaxation<sup>18</sup> using fitting parameters  $\Delta^2$ ,  $\tau_V$ ,  $\tau_M$ , its enthalpy of activation  $\Delta H_M$ , the scalar Gd- $^{17}\text{O}_w$  coupling constant  $A/h$ . Moreover, the temperature dependence of  $\tau_V$  and  $\tau_R$  has been considered using their activation energies:  $E_V$ , set to 1.0 kJ mol<sup>-1</sup>, and  $E_R$ , fixed to 18.0 kJmol<sup>-1</sup>. The best-fit parameters are listed in Table 3S and compared with those previously reported for the dimeric  $\text{Gd}_2(\text{HPADO3A})_2$  complex.<sup>19</sup>

**Table S2.** Best-fit parameters obtained from the analysis of the  $1/T_1$   $^1\text{H}$  NMRD profiles (298 and 310 K) and  $^{17}\text{O}$  NMR data for Gd(HPADO3A), Gd(BzHPADO3A), Gd(PipHPADO3A) and  $\text{Gd}_2(\text{HPADO3A})_2$ <sup>19</sup>

Parameter <sup>a</sup>	GdHPA- DO3A (pH 4.2)	GdHPADO3A (pH 7.4)	GdBzHPADO3A (pH 4.2)	GdBzHPADO3A (pH 7.4)	GdPipHPA- DO3A (pH 4.2)	GdPipHPA- DO3A (pH 7.4)	$\text{Gd}_2(\text{HPA-DO3A})_2$
$^{20}r_1^{298}$ ( $\text{mM}^{-1} \text{s}^{-1}$ )	$9.8 \pm 0.2$	$4.3 \pm 0.1$	$7.2 \pm 0.1$	$4.5 \pm 0.1$	$5.3 \pm 0.2$	$4.6 \pm 0.1$	9.5
$^{20}r_{1\text{-seronorm}}^{298}$ ( $\text{mM}^{-1} \text{s}^{-1}$ )	--	$6.7 \pm 0.1$	--	$7.7 \pm 0.1$	--	$8.5 \pm 0.1$	--
$r_{1\text{pr}}^{298}$ ( $\text{mM}^{-1} \text{s}^{-1}$ )	$4.99 \pm 0.02$	--	$2.87 \pm 0.02$	--	$1.12 \pm 0.03$	--	--
$\Delta^2$ ( $10^{19} \text{s}^{-2}$ )	$12.0 \pm 0.7$	$8.5 \pm 1.1$	$6.8 \pm 1.6$	$10.2 \pm 1.4$	$10.1 \pm 1.0$	$3.5 \pm 0.9$	6.2
$\tau_V^{298}$ (ps)	$4.5 \pm 0.6$	$13.8 \pm 0.8$	$5.0 \pm 1.1$	$13.1 \pm 0.9$	$10.4 \pm 0.7$	$25.2 \pm 1.5$	22
$\tau_M^{298}$ (ns)	$24.5 \pm 0.5$	$20.2 \pm 2.4$	21.6 <sup>c</sup>	$24.2 \pm 2.1$	21.6 <sup>c</sup>	$45.0 \pm 1.4$	5.0
$\tau_R^{298}$ (ps)	$62.0 \pm 1.2$	$62.0 \pm 1.3$	$70.8 \pm 2.1$	$70.8 \pm 1.5$	$82.2 \pm 1.5$	$82.2 \pm 2.0$	140
$\Delta H_M$ (kJ/mol)	$15.5 \pm 0.7$	$14.9 \pm 1.7$	--	$13.0 \pm 0.5$	--	$7.5 \pm 0.3$	29.5
$A/h$ ( $10^6 \text{rad s}^{-1}$ )	$-3.4 \pm 0.1$	$-3.4 \pm 0.1$	-3.4 <sup>c</sup>	$-3.4 \pm 0.1$	-3.4 <sup>c</sup>	$-3.4 \pm 0.1$	$-3.4 \pm 0.1$
$q^{\text{ss}}$	5	5	4	4	3	3	4
$\tau_R^{\text{sf}}$ (ps)	$30.0 \pm 2.5$	$12.7 \pm 0.9$	$24.5 \pm 2.1$	$23.2 \pm 1.0$	$24.0 \pm 1.3$	$10.1 \pm 0.9$	60

<sup>a</sup> The parameters fixed in the fitting procedure are:  $q = 1$ ,  $r_{\text{GdO}} = 2.5 \text{ \AA}$ ,  $r_{\text{GdH}} = 3.0 \text{ \AA}$ ,  $a_{\text{GdH}} = 4.0 \text{ \AA}$ ,  $^{298}D_{\text{GdH}} = 2.25 \times 10^{-5} \text{ cm}^2 \text{ s}^{-1}$ ,  $E_R = 18 \text{ kJ mol}^{-1}$ ,  $E_V = 1 \text{ kJ mol}^{-1}$ ,  $r_{\text{GdH(SS)}} = 3.5 \text{ \AA}$ ; <sup>c</sup>These values were also fixed considering the data obtained by fitting the profiles at pH 4.2 for Gd(HPADO3A).

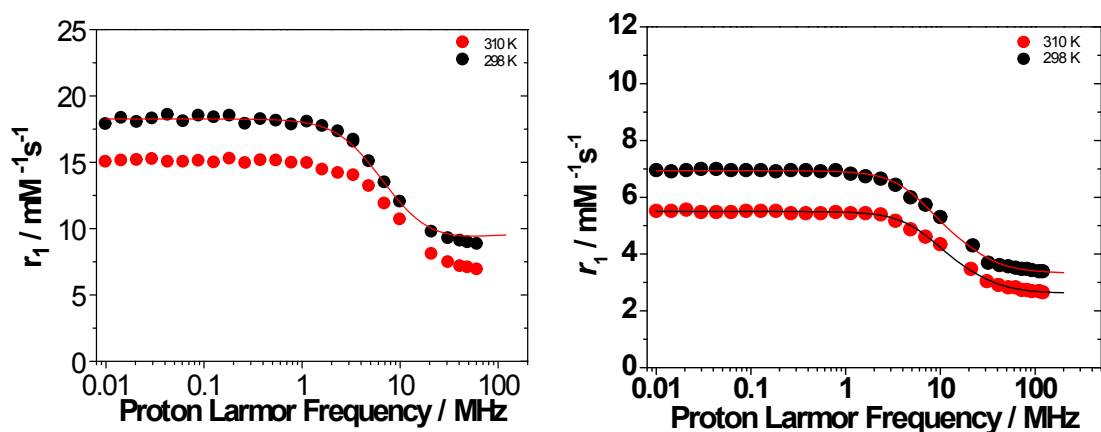


**Figure S7.**  $^1\text{H}$  NMRD profiles of Gd(HPADO3A) at 298 and 310 K at pH 4.2 (left) and 7.4 (right). The solid lines represent the best fitting results of the experimental data points with the parameters in Table S2.

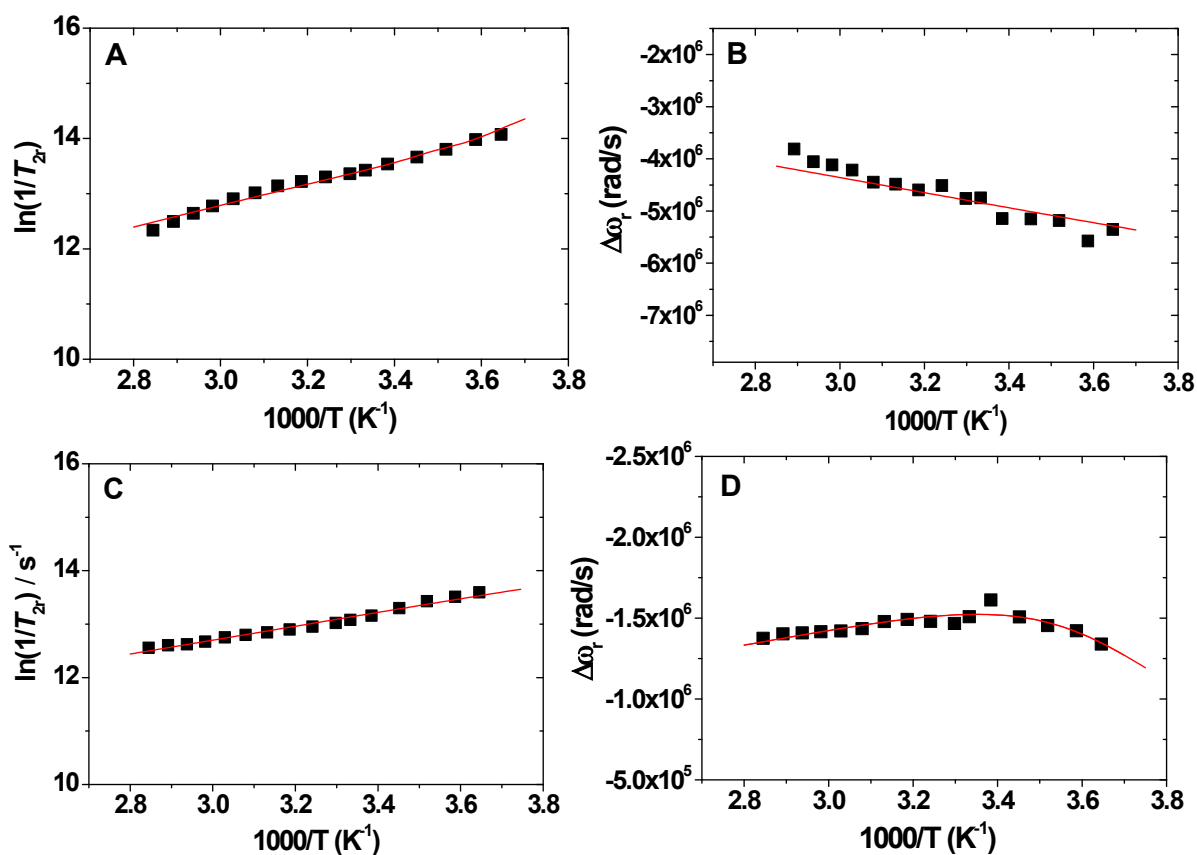


**Figure S8.** Reduced transverse  $^{17}\text{O}$  relaxation rates (A and C) and chemical shifts (B and D) measured at 11.74 T for Gd(HPADO3A) at pH 4.2 (top) and 7.4 (bottom). The solid lines correspond to the fits of the data as described in the text.

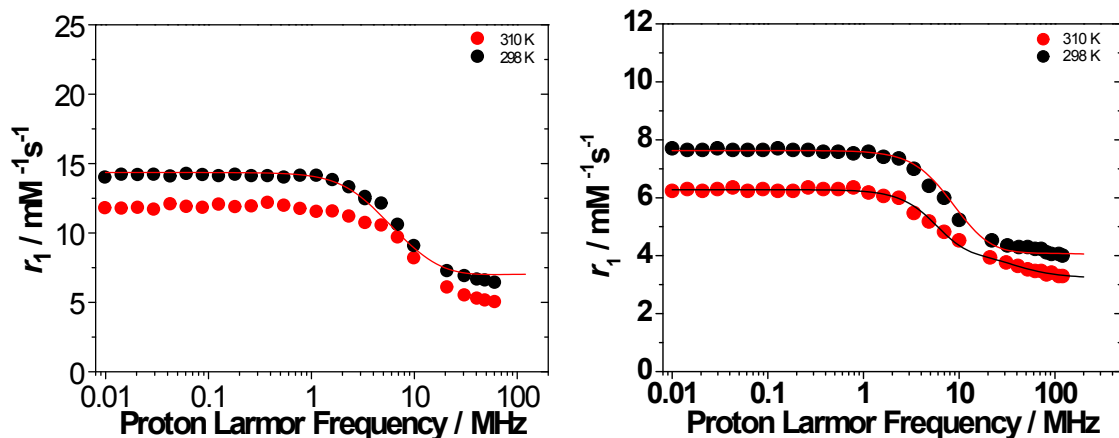


**Figure S9.**  $^1\text{H}$  NMRD profiles of Gd(BzHPADO3A) at 298 and 310 K at pH 4.2 (left) and 7.4 (right). The solid lines represent the best fitting results of the experimental data points with the parameters in Table S2.

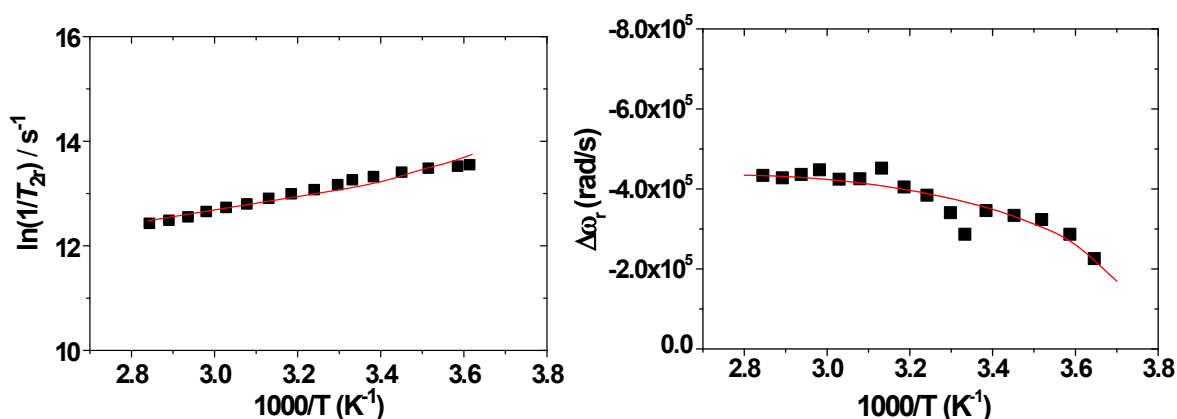


**Figure S10.** Reduced transverse  $^{17}\text{O}$  relaxation rates (left) and chemical shifts (right) measured at 11.74 T for Gd(BzHPADO3A) at pH 7.4. The solid lines correspond to the fits of the data as described in the text.

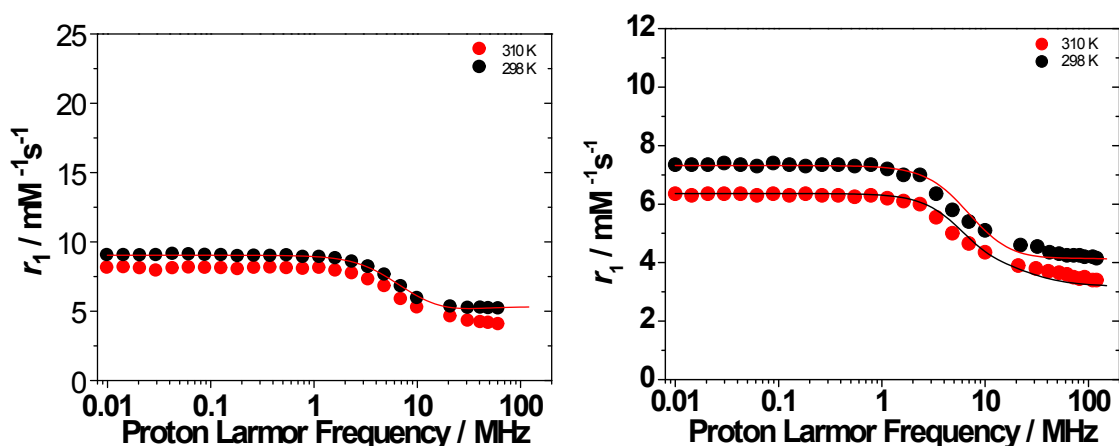


**Figure S11.**  $^1\text{H}$  NMRD profiles of Gd(PipHPADO3A) at 298 and 310 K at pH 4.2 (left) and 7.4 (right). The solid lines represent the best fitting results of the experimental data points with the parameters in Table S2.

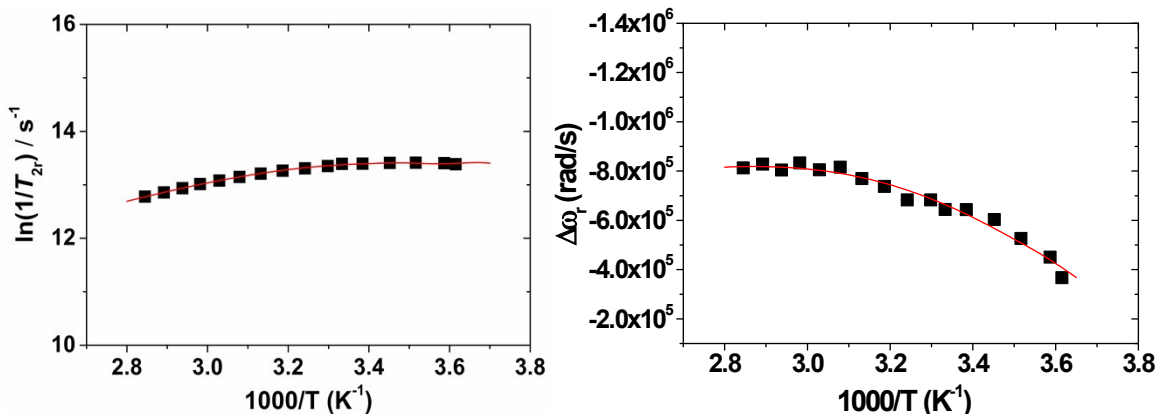


**Figure S12.** Reduced transverse  $^{17}O$  relaxation rates (left) and chemical shifts (right) measured at 11.74 T for Gd(PipHPADO3A) at pH 7.4. The solid lines correspond to the fits of the data as described in the text.

## VI. Chemical Exchange Saturation Transfer (CEST)-MRI study

### VI.1. Experimental: CEST-MRI

In order to get further insight into the mechanism of the acid-base catalyzed proton exchange process, Chemical Exchange Saturation Transfer Magnetic Resonance imaging (CEST- MRI) of Eu(HPADO3A), Yb(HPADO3A), Eu(Bz-HPADO3A) and Eu(Pip-HPADO3A) was carried out. MR images were acquired on phantoms composed by glass capillaries filled with aqueous solutions of the paramagnetic complexes at different pH in a range between 4.5 and 10.0, at 21°C. MR images were acquired at 7T by using a Bruker Avance 300 spectrometer equipped with a microimaging probe. A frequency offset range of  $\pm 200$  ppm was investigated. A typical RARE spin-echo sequence with TE 3 ms, TR 5 s and RARE factor 16 was used. An isotropic  $64 \times 64$  acquisition matrix with a FOV of 10 mm and a slice thickness of 1 mm was used (spatial resolution =  $156 \times 156 \mu m^2$ ). The whole sequence was preceded by a saturation scheme consisting of a continuous rectangular wave pulse 2 s long with a radiofrequency  $B_1$  field of 12  $\mu T$  for Eu<sup>III</sup>-complexes and 24  $\mu T$  for Yb<sup>III</sup>-complex. The Z-spectra were interpolated by smoothing splines to identify the zero-offset on a pixel-by-pixel basis of the bulk water and, then, to assess the correct ST % value over the entire range of frequency offsets investigated. Custom-made software, compiled in the Matlab platform (Mathworks Inc., Natick, MA), was used.<sup>20</sup> The extent of CEST effect was calculated as follows:

$$ST\% = \left(1 - \frac{M_s}{M_0}\right) \times 100 \quad (17)$$

where  $M_s$  is the intensity of the bulk water NMR signal after the irradiation on resonance ( $\Delta\omega$ ) of the mobile proton pool and  $M_0$  is the intensity of the bulk water NMR signal after the irradiation at the opposite frequency ( $-\Delta\omega$ ).

### VI.2. CEST-MRI

CEST experiments of Yb(HPADO3A) solutions at variable pH are reported in Figure S13. For a 6 mM water solution of Yb(HPADO3A), the CEST peak is present at 80 ppm, with a ST% that decreases from *ca.*13% at pH = 4.5 to *ca.*1% at pH = 7.5 ( $B_1 = 12 \mu T$ ) (Figure S13).

Representative CEST-MR images of phantoms containing glass capillaries filled with Yb(HPADO3A) at variable pH are reported in Figure S14.

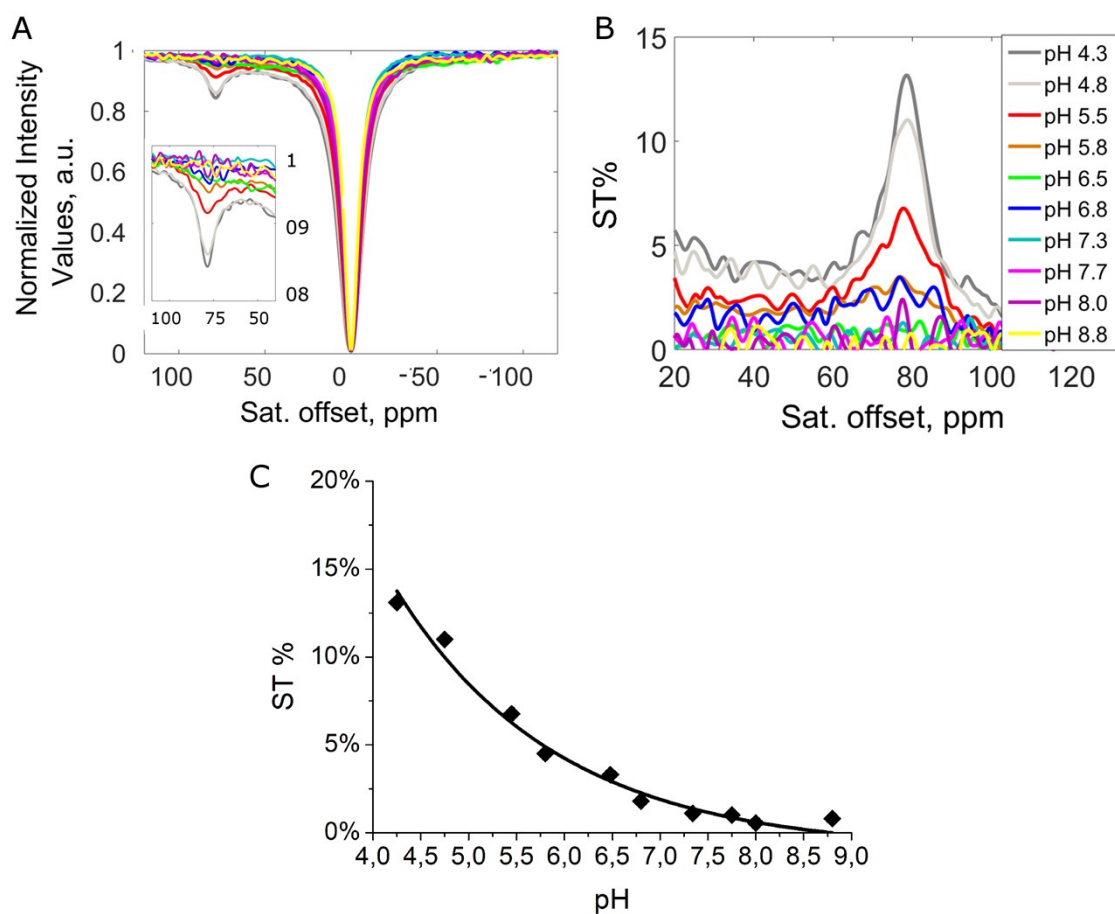


**Figure S13.** (A) Z-spectra and (B) St%-spectra of Yb(HPADO3A) (6mM) in water at different pHs; (C) ST% effect for Yb(HPADO3A), in water as a function of pH.

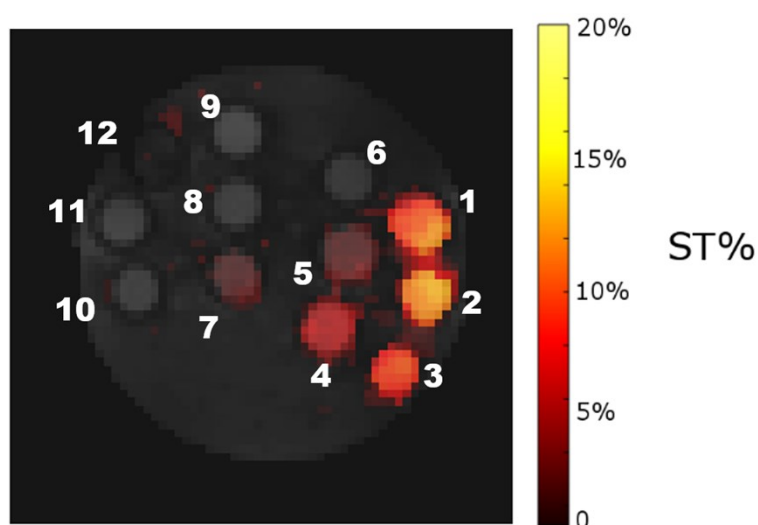


**Figure S14.** ST-weighted CEST map capillaries filled with Yb(HPADO3A) (6mM) in water at various pH values (Legend: 1=pH 4.3; 2=pH 4.8; 3=pH 5.5; 4=pH 5.8; 5=pH 6.5; 6=pH 6.8; 7=pH 7.3; 8=pH 7.8; 9=pH 8.0; 10= pH 8.8; 11=water; 12= buffer).

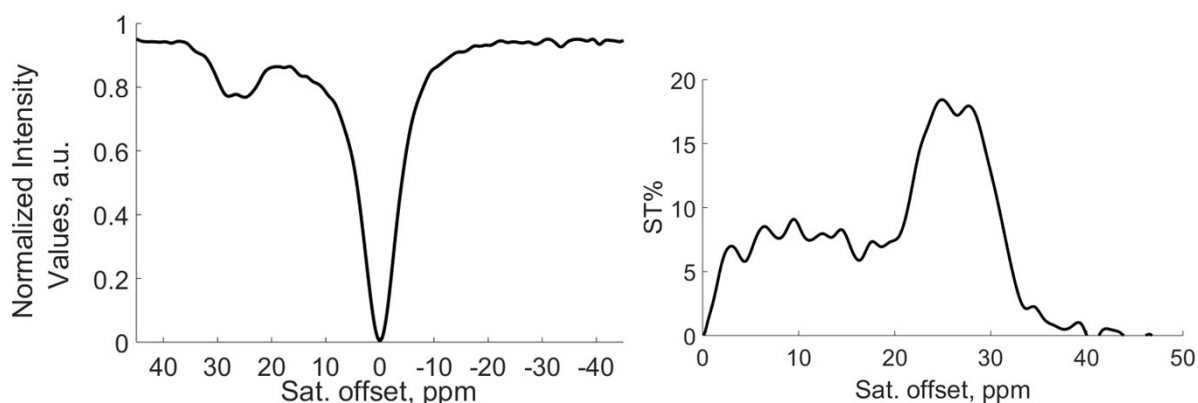


**Figure S15.** (*left*) Z-spectrum and (*right*) ST-spectrum of EuHPADO3A (pH = 4.5, T = 298 ± 2 K, B<sub>1</sub> = 6 μT)

By using higher B<sub>1</sub> fields (*e.g.* 12 μT as used previously) there is a broadening of the signals that are not yet clearly distinguishable. An asymmetric peak centered at 27 ppm is present. Also by increasing the temperature up to RT and by using a B<sub>1</sub>=12 μT (the parameters used for all the other experiments reported in the paper), there is an increase of exchange rate and the coalescence of the two peaks with only one CEST signal present.

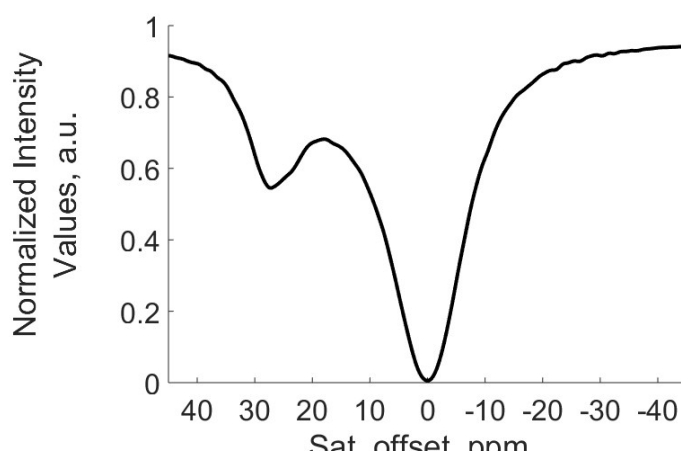


**Figure S16.** Z-spectrum of EuHPADO3A (pH = 4.5, T = 298 ± 2 K, B<sub>1</sub>=12 μT)

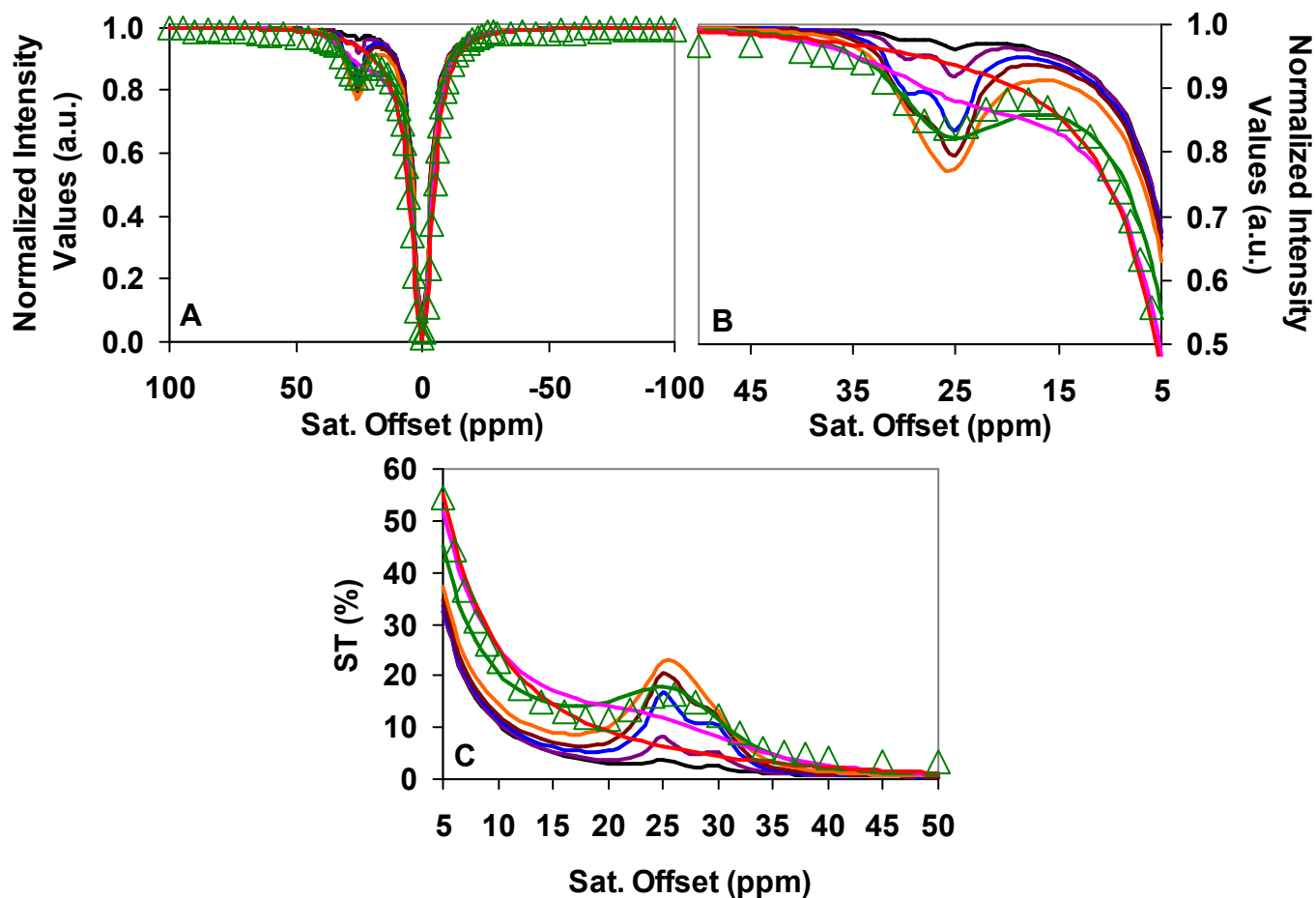


**Figure S17.** Simulated Z-spectra (A and B) and ST spectra (C) of Eu(HPADO3A) by considering a three-pool exchange system with bulk water (pool A) at zero, -OH (pool B) at 30 and  $-\text{NH}_2$  (pool C) at 25 ppm. Open symbols and solid lines represent the experimental and the calculated ST values, respectively. Simulations have been performed by using Bloch equations modified for chemical exchange as it is described in Ref. [21]. Parameters used in these simulations:  $B_0=300$  MHz,  $B_1=512$  Hz,  $t_{\text{sat}}=2$  s,  $c_A=111$  M,  $c_B=0.02$  M,  $c_C=0.04$  M,  $T_{1a}=0.7$  s,  $T_{2a}=0.1$  s,  $T_{1b}=T_{2b}=T_{1c}=T_{2c}=0.006$  s,  $\tau_{BA}=\tau_{CA}=\tau_{BC}=\mathbf{10, 3, 1, 0.6, 0.3, 0.1, 0.06}$  and  $\mathbf{0.05}$  ms.

In the case of the secondary amide derivative Eu(Bz-HPADO3A) the CEST experiments at variable pH are reported in Figure S15. Again, only one CEST peak is present at 25 ppm with a ST% reducing to almost zero moving from acidic to basic pH. On the other hand, CEST experiments on 16 mM Eu(Pip-HPADO3A) solutions at variable pH, reported in Figure S16, do not display a clear CEST signal in the 25 ppm region.

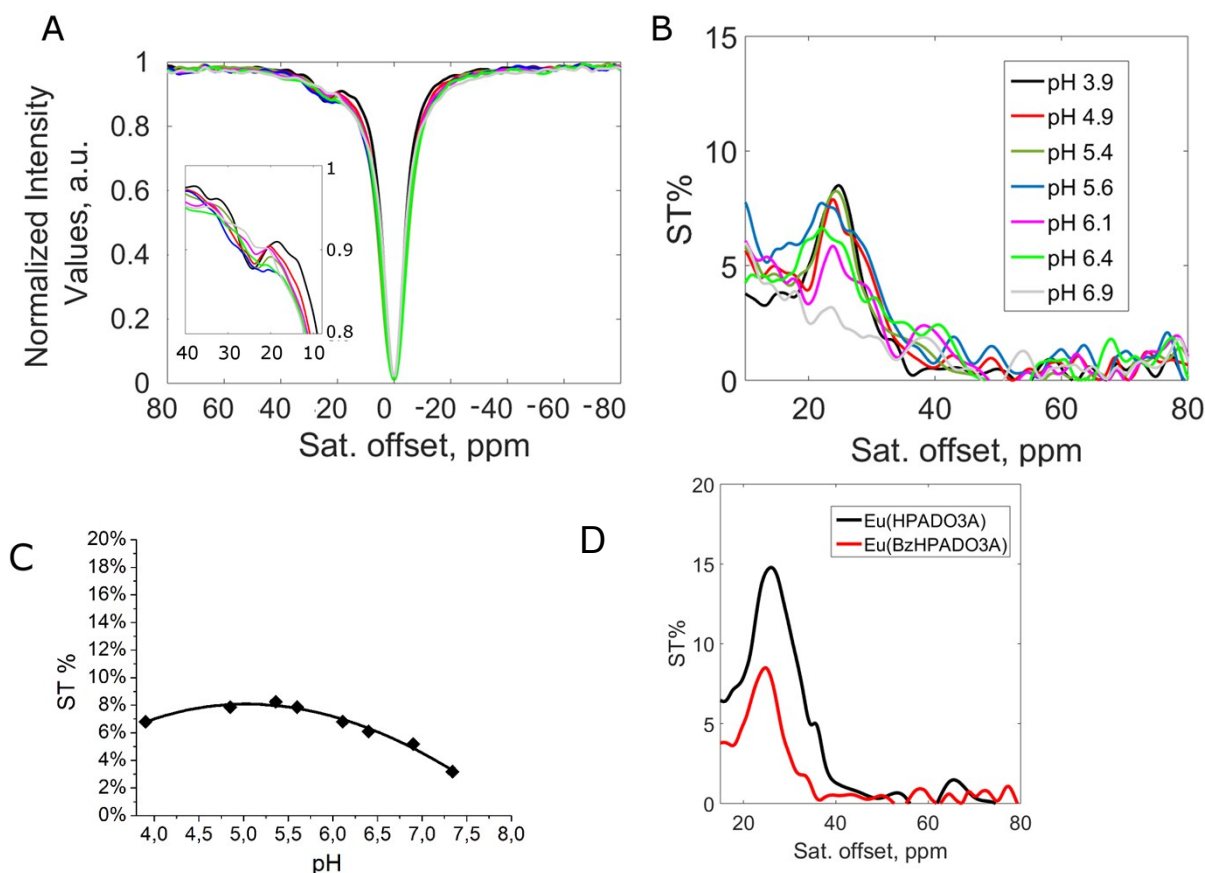


**Figure S18** (A) Z-spectra and (B) St%-spectra of Eu(Bz-HPADO3A) (20mM) in water at different pH; (C) ST% effect for Eu(Bz-HPADO3A), in water as a function of pH; (D) comparison between ST% effects of Eu(HPADO3A) (black) and Eu(Bz-HPADO3A) (red) measured in the same experimental conditions.

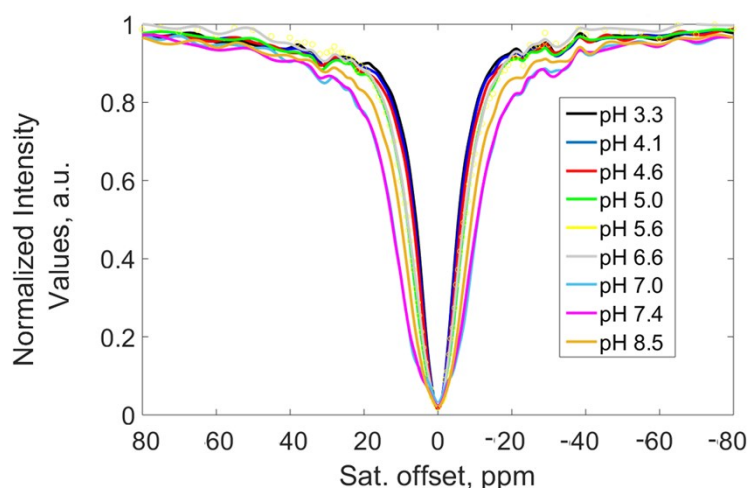


**Figure S19.** Z-spectra of Eu(Pip-HPADO3A) solutions(16mM) in water as a function of pH.

## VII. References

- 1 H. M. Irving, M. G. Miles, L. D. Pettit, *Anal. Chim. Acta* 1967, **38**, 475.
- 2 L. Zekany, I. Nagypal, I. In *Computational Methods for the Determination of Formation Constants*; Leggett, D., Ed.; Springer US: 1985, p 291.
- 3 J. F. Desreux, E. Merciny, M. F. Loncin, *Inorg. Chem.* 1981, **20**, 987.; A. Bianchi, L. Calabi, C. Giorgi, P. Losi, P. Mariani, P. Paoli, P. Rossi, B. Valtancoli, M. Virtuani, *J. Chem. Soc., Dalton Trans.* 2000, 697.; A. Takács, R. Napolitano, M. Purgel, A. C. Bényei, L. Zékány, E. Brücher, I. Tóth, Z. Baranyai, S. Aime, *Inorg. Chem.* 2014, **53**, 2858.
- 4 E. T. Clarke, A. E. Martell, *Inorg. Chim. Acta* 1991, **190**, 27.
- 5 W. P. Cacheris, S. K. Nickle, A. D. Sherry, A. D. *Inorg. Chem.* 1987, **26**, 958.
- 6 K. Kumar, M. F. Tweedle, M. F.; Malley, J. Z. Gougoutas, *Inorg. Chem.* 1995, **34**, 6472.
- 7 E. Tóth, R. Kiraly, J. Platzek, B. Raduchel. E. Brucher, *Inorg Chim Acta* 1996, **249**, 191-199.
- 8 a) É. Tóth, E. Brücher, I. Lázár, I. Tóth, *Inorg. Chem.*, 1994, **33**, 4070.; b) S. L. Wu, W. D. Horrocks, *Inorg. Chem.*, 1995, **34**, 3724.; c) L. Burai, I. Fábíán, R. Király, E. Szilágyi, E. Brücher, *J. Chem. Soc., Dalton Trans.* 1998, 243-248 ; d) J. Moreau, E. Guillon, J. C. Pierrard, J. Rimbault, M. Port, M. Aplincourt, *Chem. Eur. J.*, 2004, **10**, 5218.
- 9 E. Prenesti, P. G. Daniele, S. Berto, S. Toso, *Polyhedron*, 2006, **25**, 2815.
- 10 A. Riesen, M. Zehnder, T. A. Kaden, *Helv. Chim. Acta* 1986, **69**, 2067.
- 11 A. E. Martell, S. M. Smith, *Critical stability constants* Vol 1-5. New York: Plenum Press; 1974-1982.
- 12 R. Delgado and J.J.R.F. Da Silva, *Talanta*, 1982, **29**, 815.
- 13 D. Banerjea, T. Kaden, H. Sigel, *Inorg. Chem.*, 1981, **20**, 2586.
- 14 S. Aime, S. Baroni, D. Delli Castelli, E. Brucher, I. Fabian, S. C. Serra, A. Fringuello Mingo, R. Napolitano, L. Lattuada, F. Tedoldi, Z. Baranyai, *Inorg. Chem.* 2018, **57**, 5567.
- 15 D.M. Corsi, C. Platas Iglesias, H. van Bekkum, J.A. Peters. *Magn. Res. Chem.* 2001, **11**, 723.
- 16 a) N. Solomon, N. Bloembergen, *J. Chem. Phys.* 1956, **25**, 261; b) N. Bloembergen, L. O. Morgan, *J. Chem. Phys.* 1961, **34**, 842.
- 17 J. H. Freed, *J. Chem. Phys.* 1978, **68**, 4034.
- 18 T. J. Swift, R. E. Connick, *J. Chem. Phys.* 1962, **37**, 307; b) T. J. Swift, R. E. Connick, *J. Chem. Phys.* 1964, **41**, 2553.
- 19 L. Leone, G Ferrauto, M. Cossi, M. Botta and L. Tei, *Front. Chem.* 2018, **6**, 158.
- 20 E. Terreno, J. Stancanello, D. Longo, D. D. Castelli, L. Milone, H. M. Sanders, M. B. Kok, F. Uggeri, S. Aime, *Cont. Med. Mol. Imag.*. 2009, **4**, 237.
- 21 D. E. Woessner, S. Zhang, M. E. Merritt, A. Dean Sherry, *Magn. Reson. Med.*, 2005, **53**, 790–799.

### VIII. $^1\text{H}$ and $^{13}\text{C}$ NMR spectra of protected and deprotected ligands

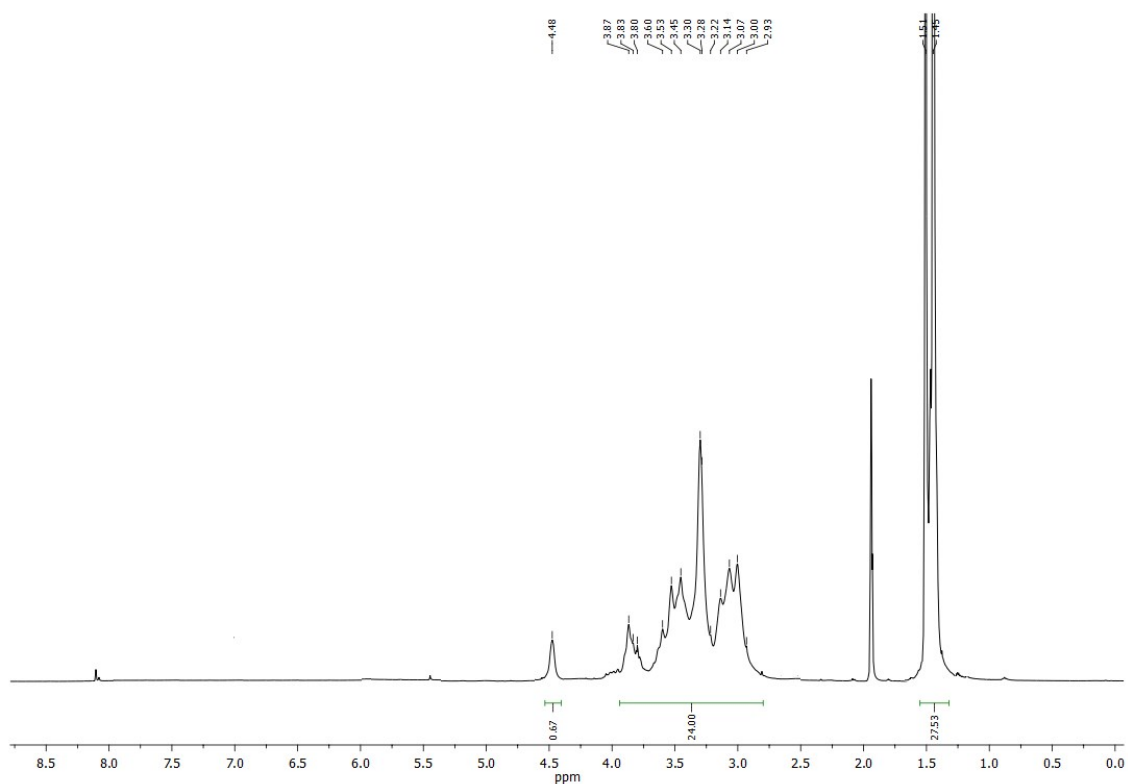


Figure S20a  $^1\text{H}$  NMR spectrum of  $\text{L1}(t\text{Bu})_3$

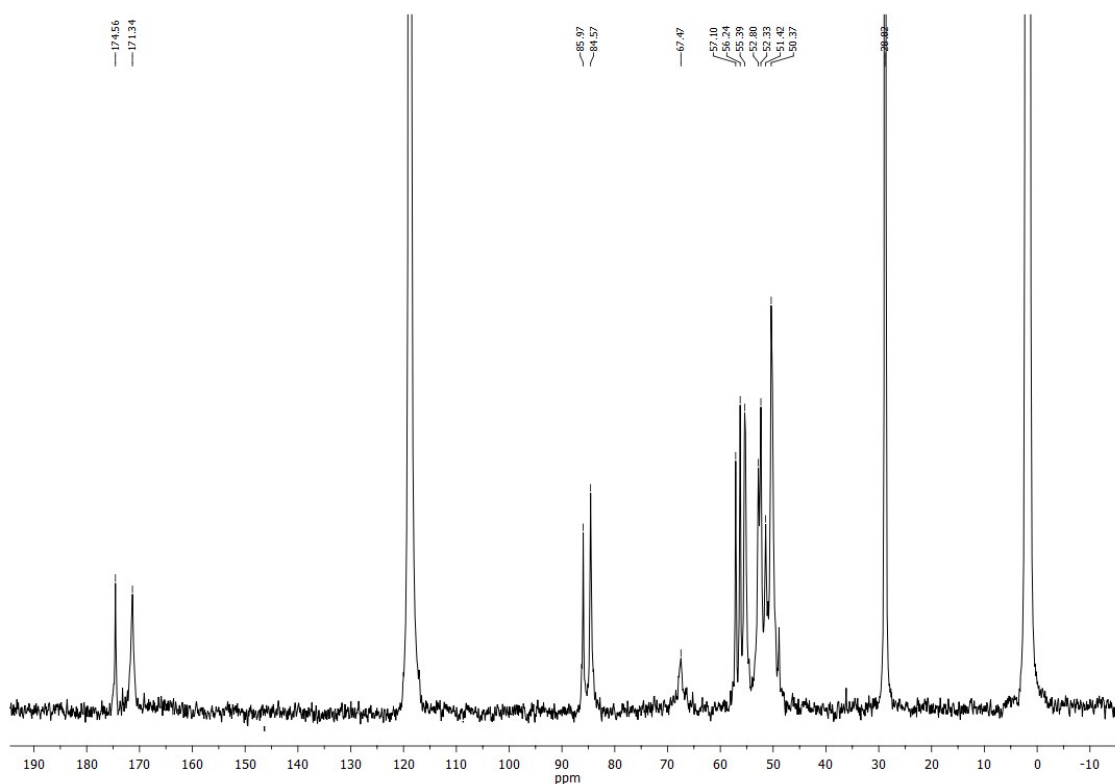


Figure S20b  $^{13}\text{C}$  NMR spectrum of  $\text{L1}(t\text{Bu})_3$

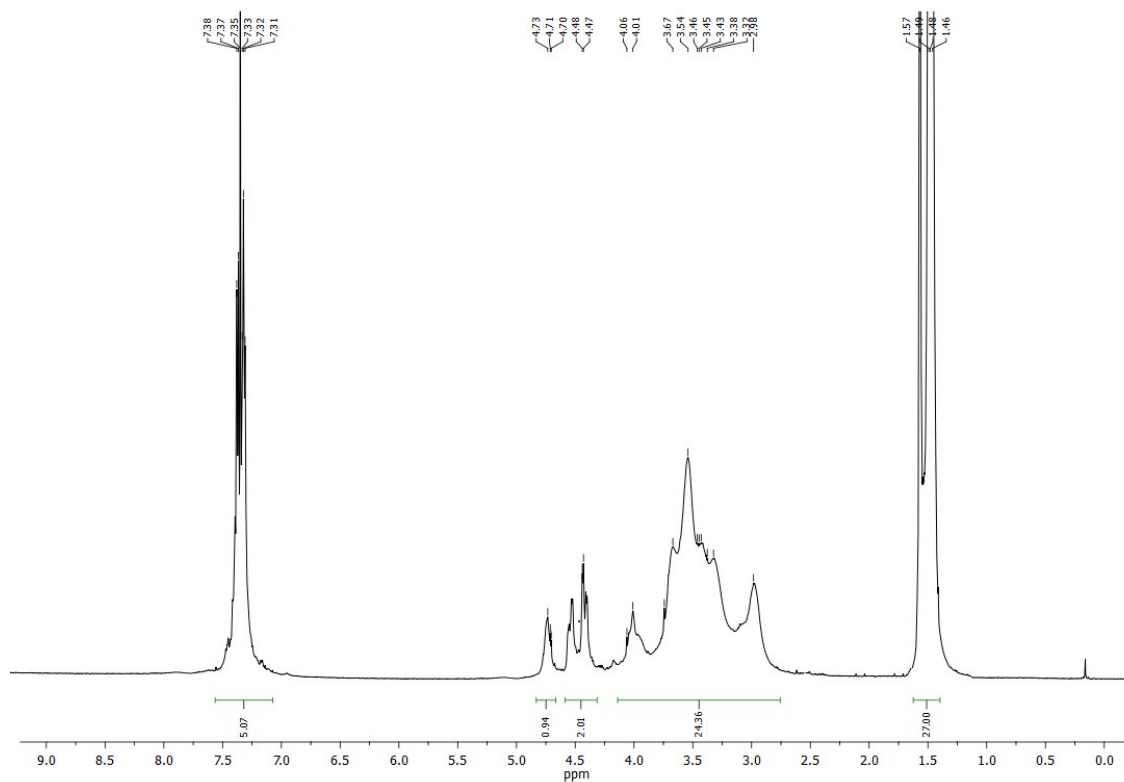


Figure S21a  $^1\text{H}$  NMR spectrum of  $\text{L2}(t\text{Bu})_3$

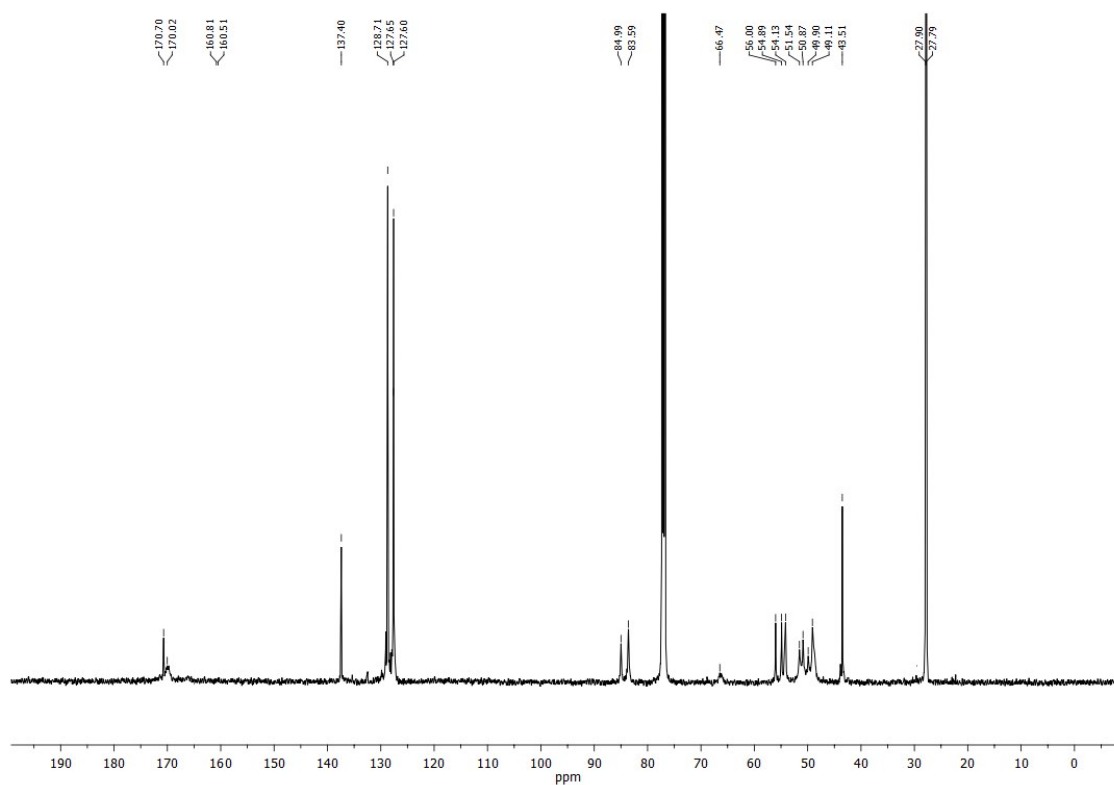


Figure S21b  $^{13}\text{C}$  NMR spectrum of  $\text{L2}(t\text{Bu})_3$

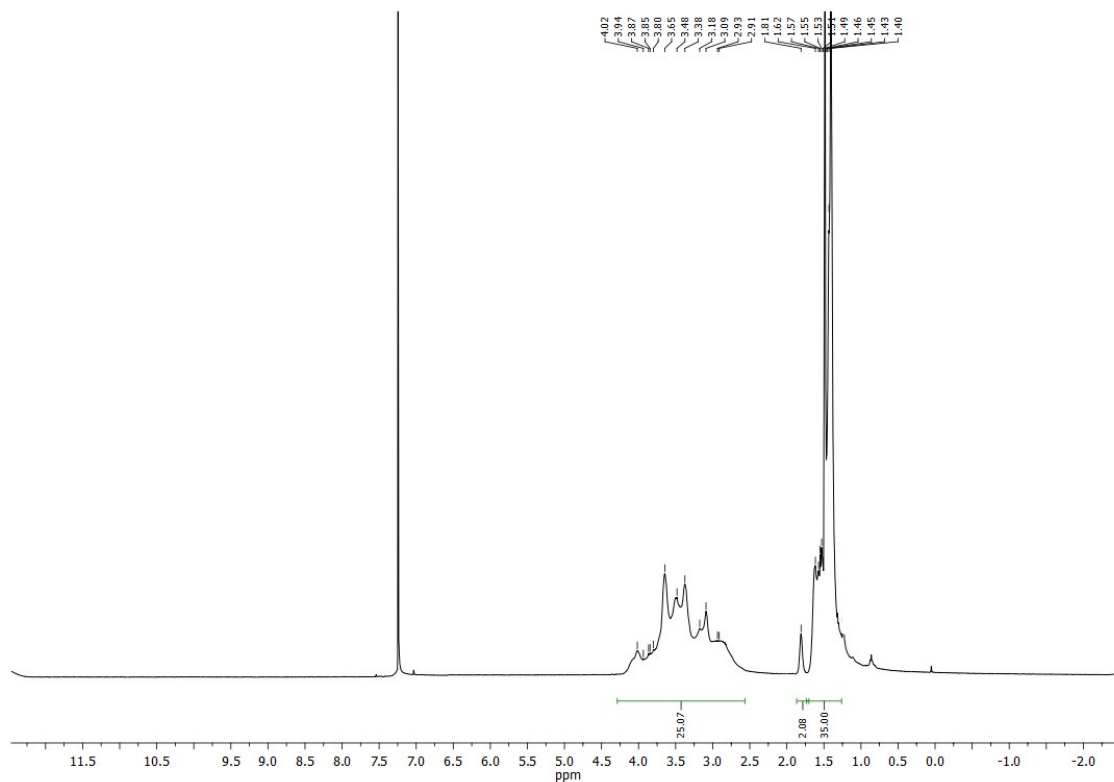


Figure S22a  $^1\text{H}$  NMR spectrum of  $\text{L3}(t\text{Bu})_3$

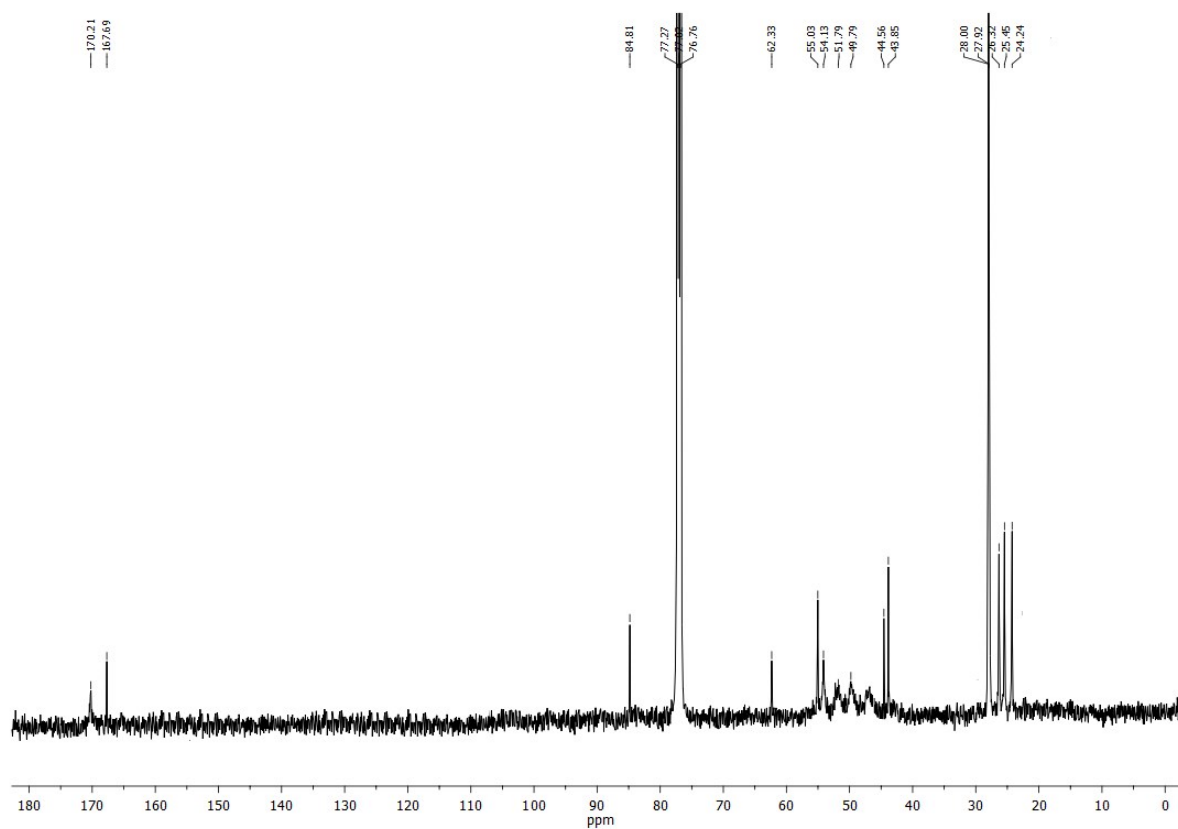
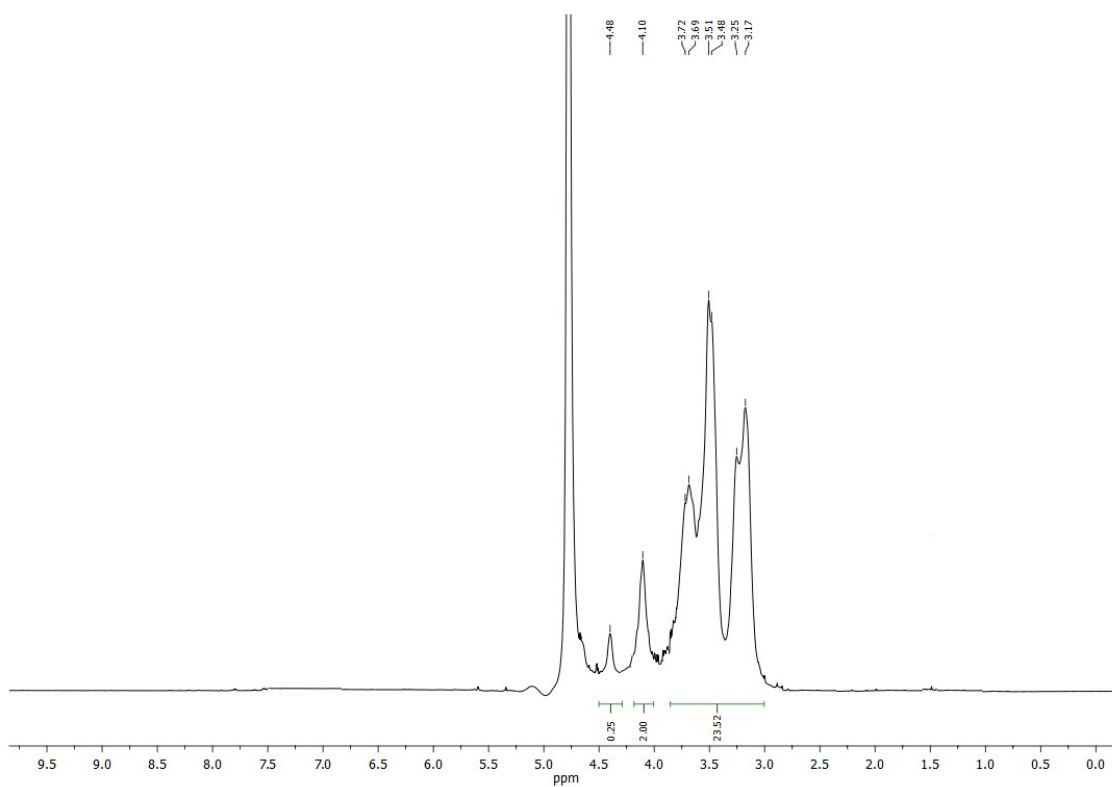
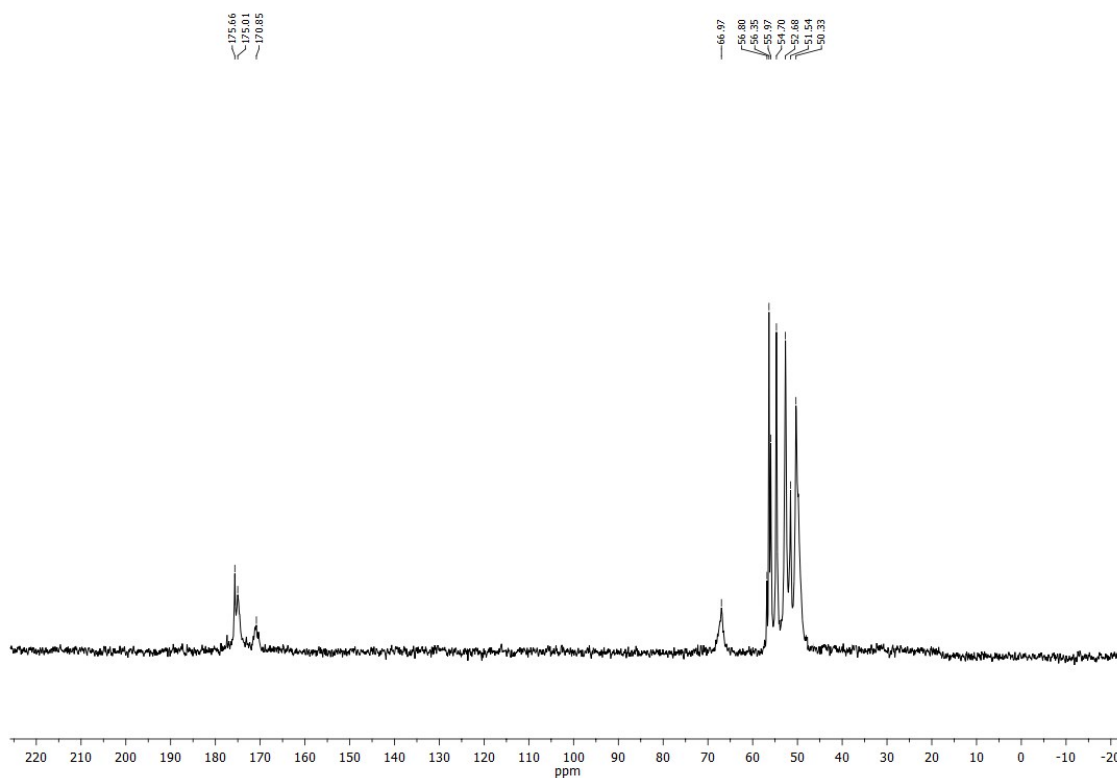


Figure S22b  $^{13}\text{C}$  NMR spectrum of  $\text{L3}(t\text{Bu})_3$



**Figure S23a**  $^1\text{H}$  NMR spectrum of HPADO3A, L1



**Figure S23b**  $^{13}\text{C}$  NMR spectrum of HPADO3A, L1

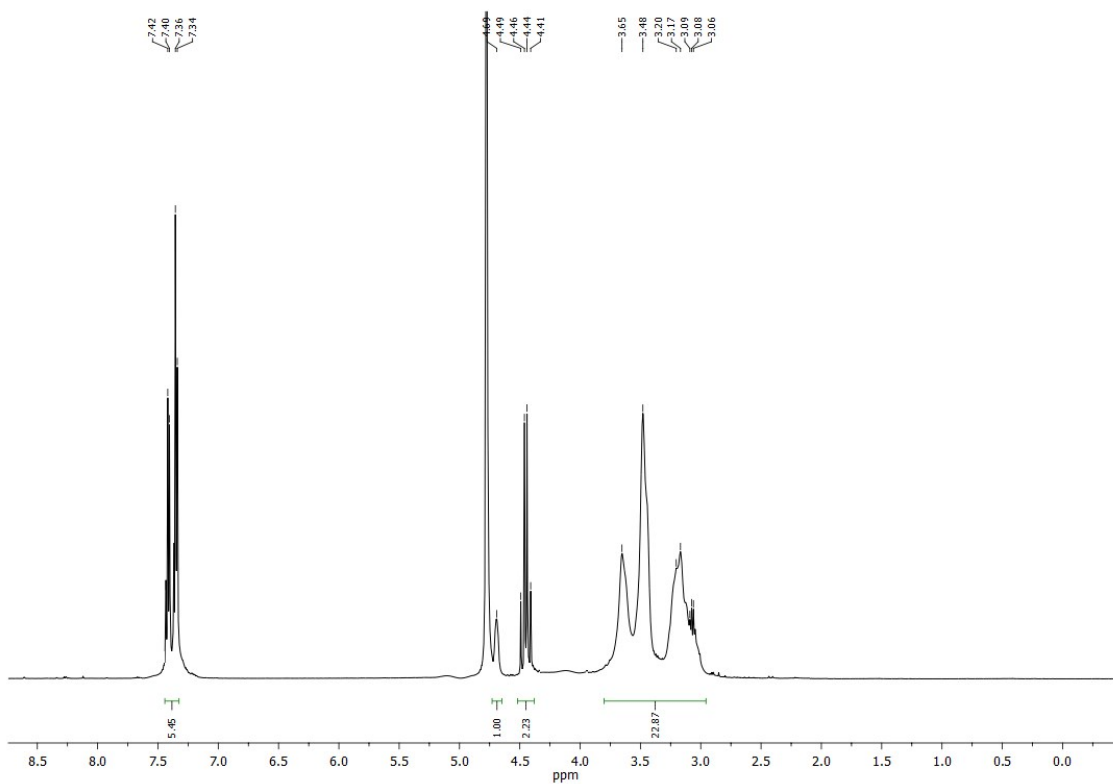


**Figure S24a**  $^1\text{H}$  NMR spectrum of BzHPADO3A, L2

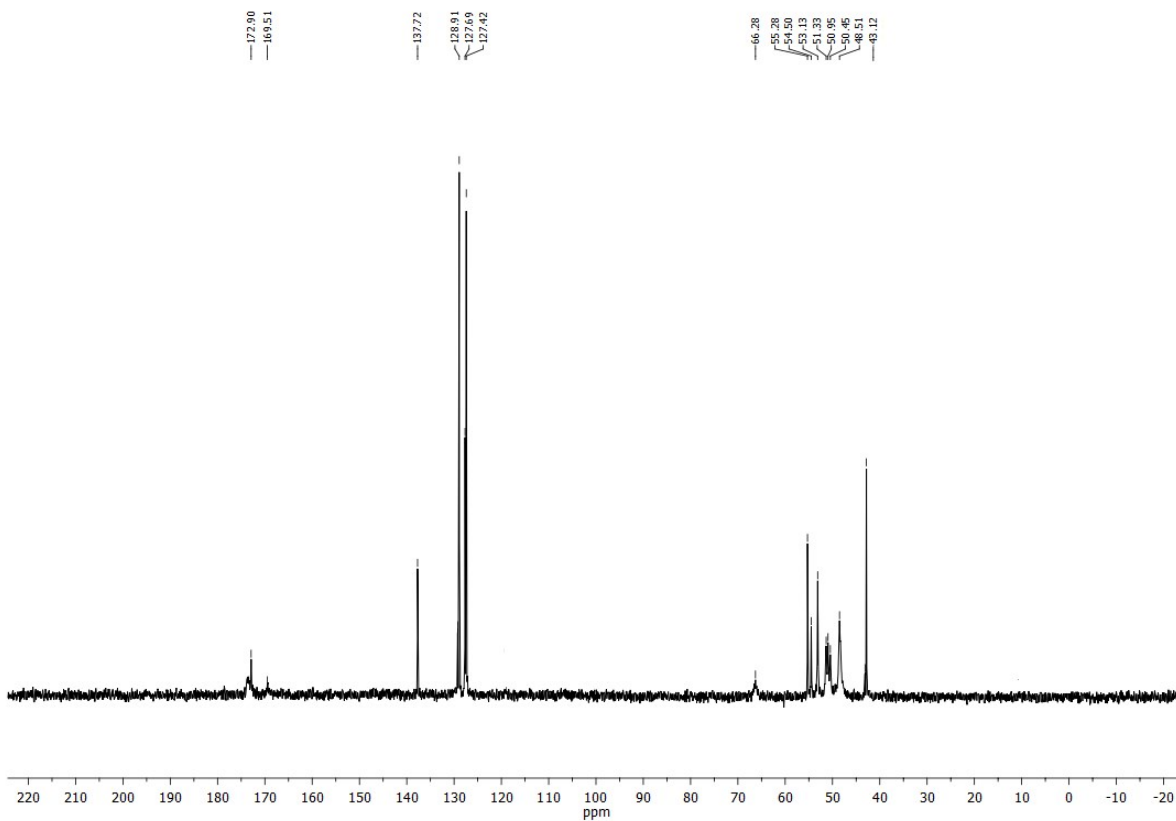


**Figure S24b**  $^{13}\text{C}$  NMR spectrum of BzHPADO3A, L2

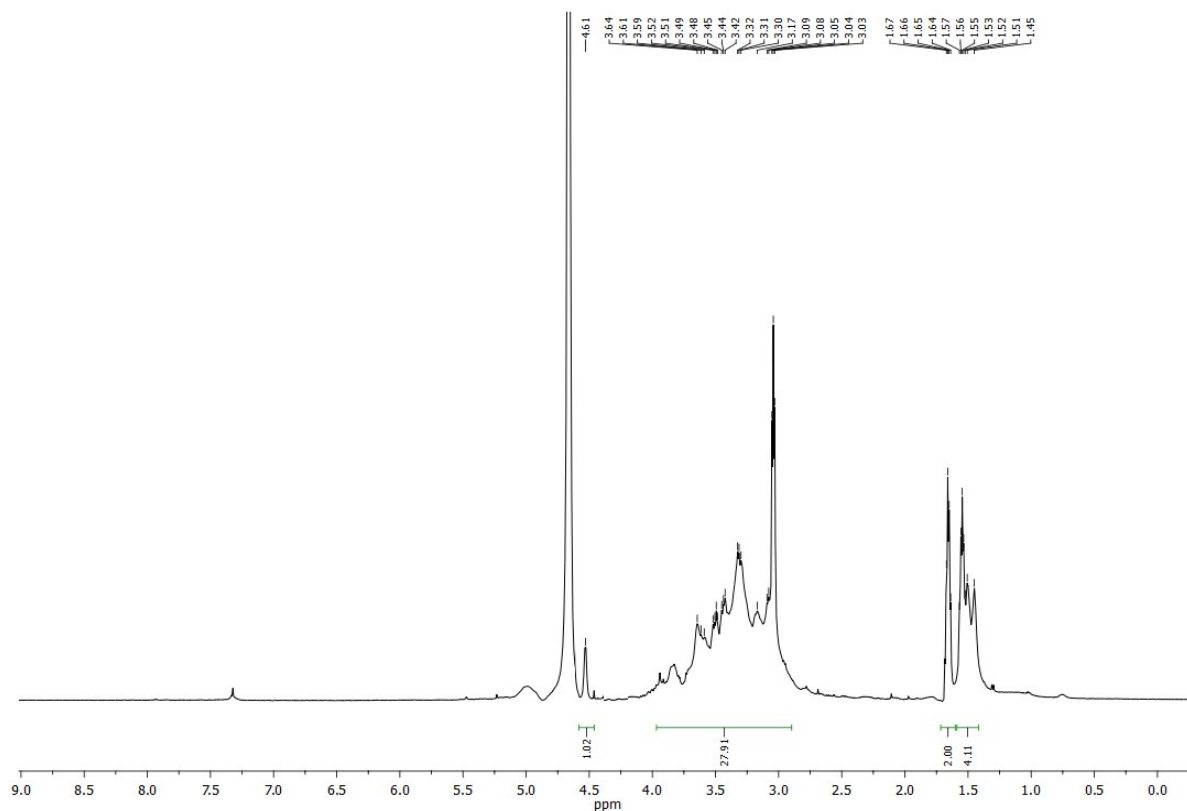


**Figure S25a**  $^1\text{H}$  NMR spectrum of PipHPADO3A, L3

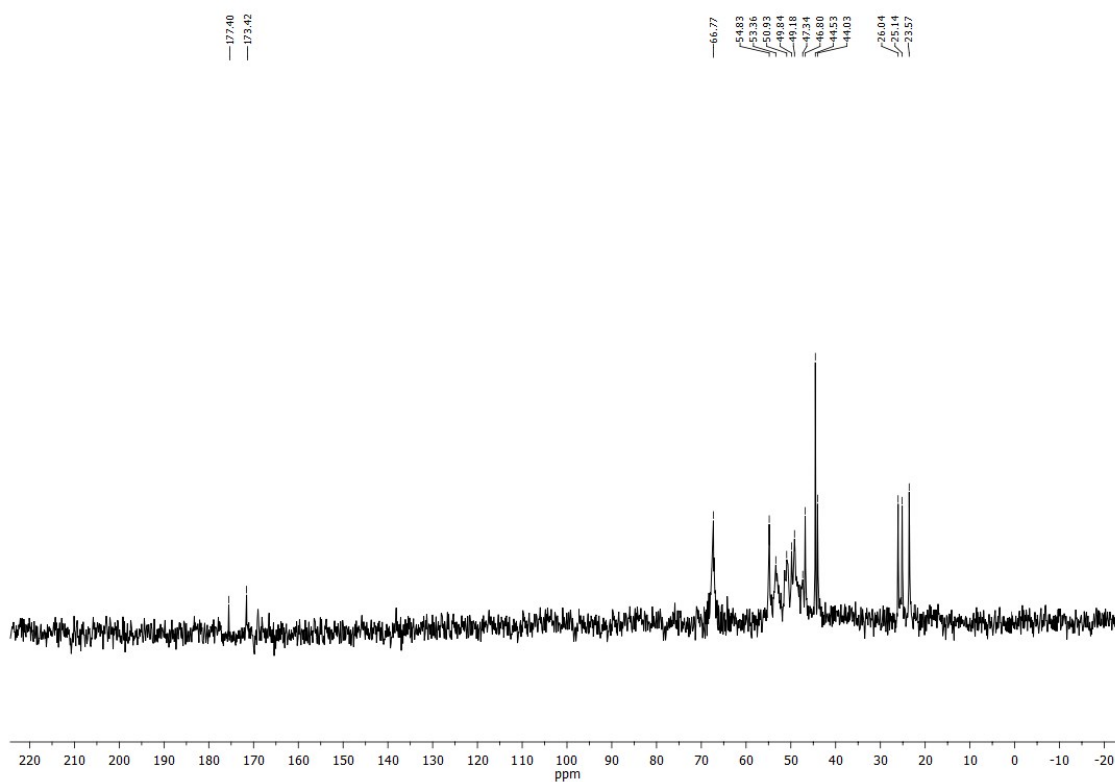


**Figure S25b**  $^{13}\text{C}$  NMR spectrum of PipHPADO3A, L3

## IX. HPLC chromatograms and ESI-MS spectra of ligands and complexes

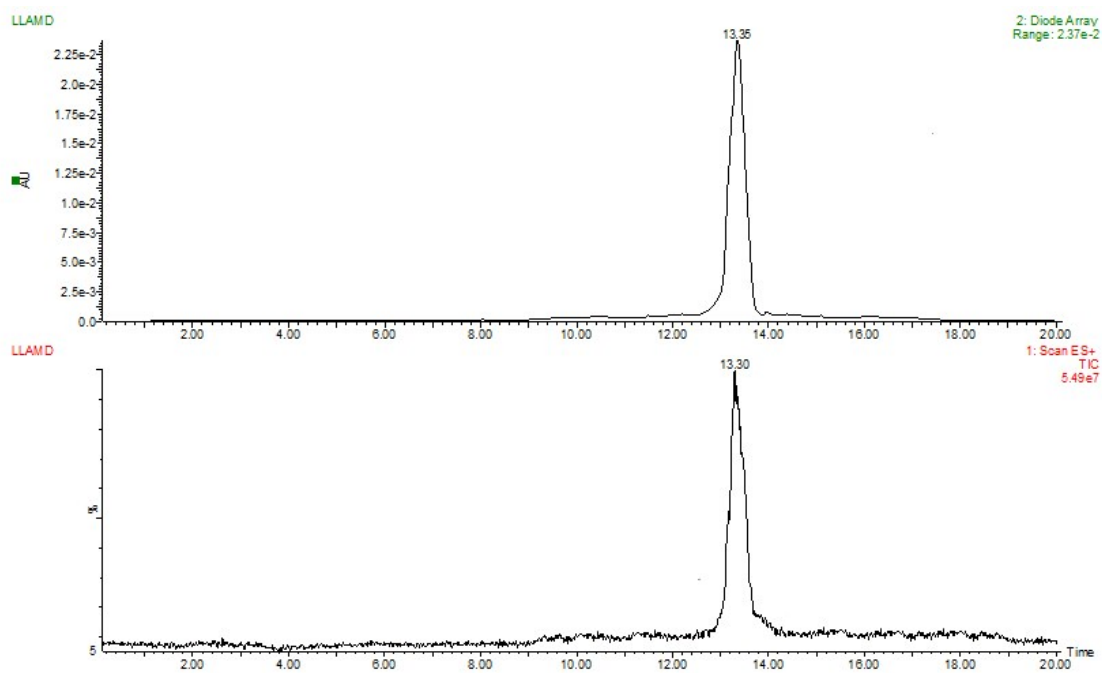


Figure S26a HPLC-MS chromatogram of HPADO3A, L1

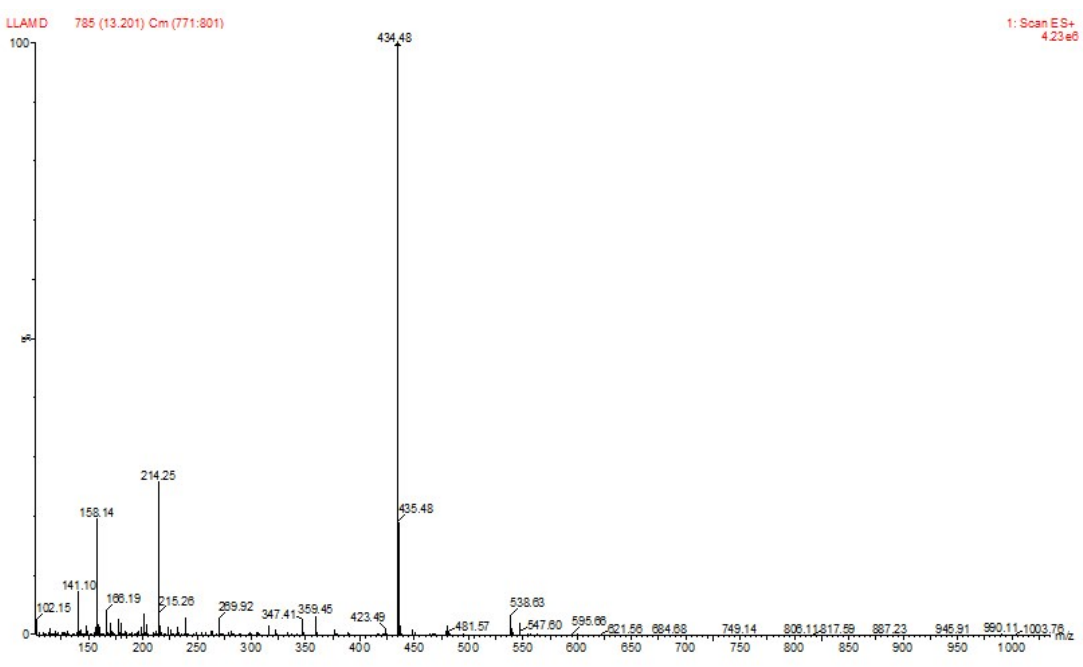


Figure S26b. ESI-MS spectrum of HPADO3A, L1

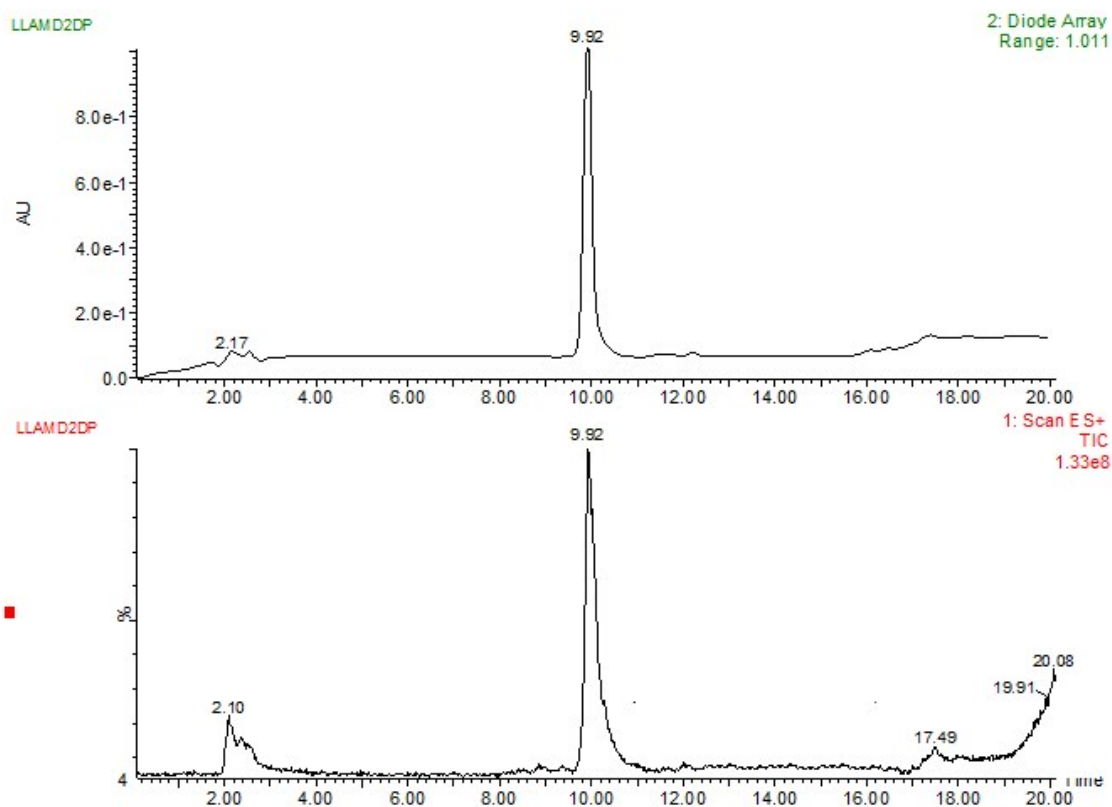


Figure S27a HPLC-MS chromatogram of BzHPADO3A, L2

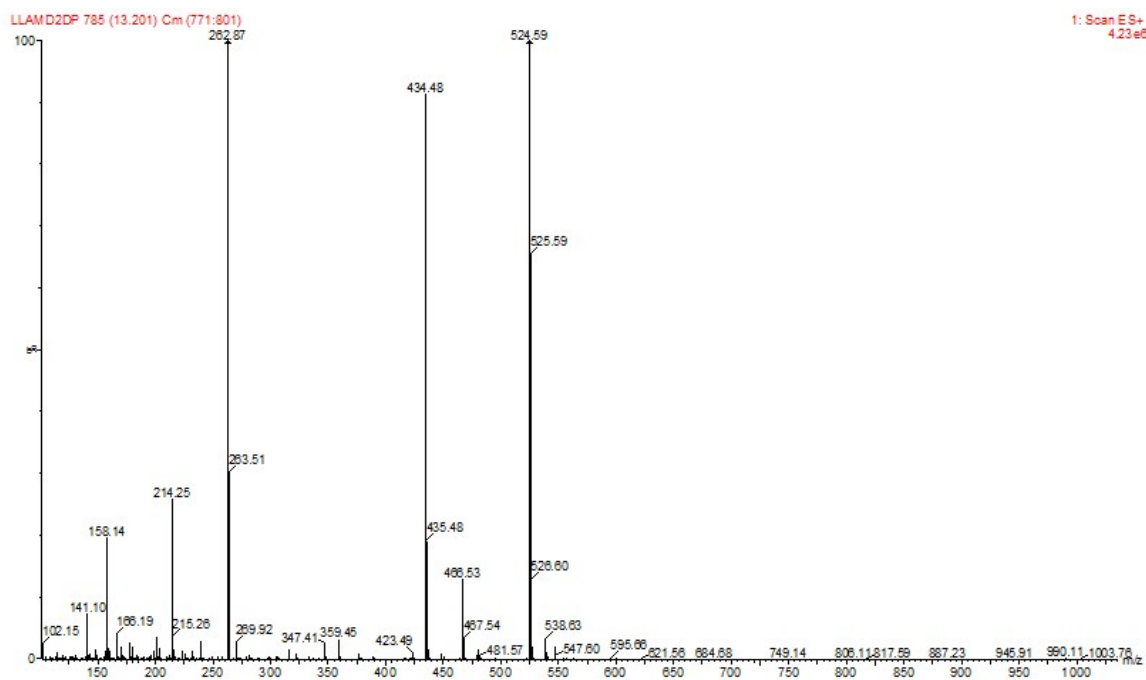
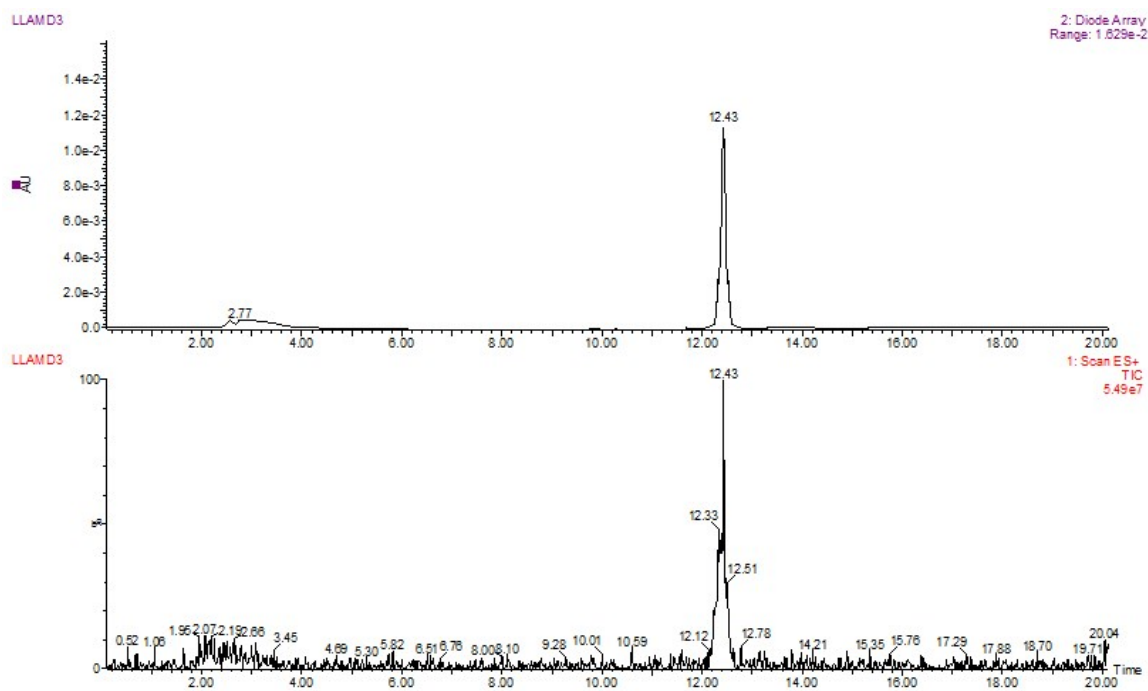
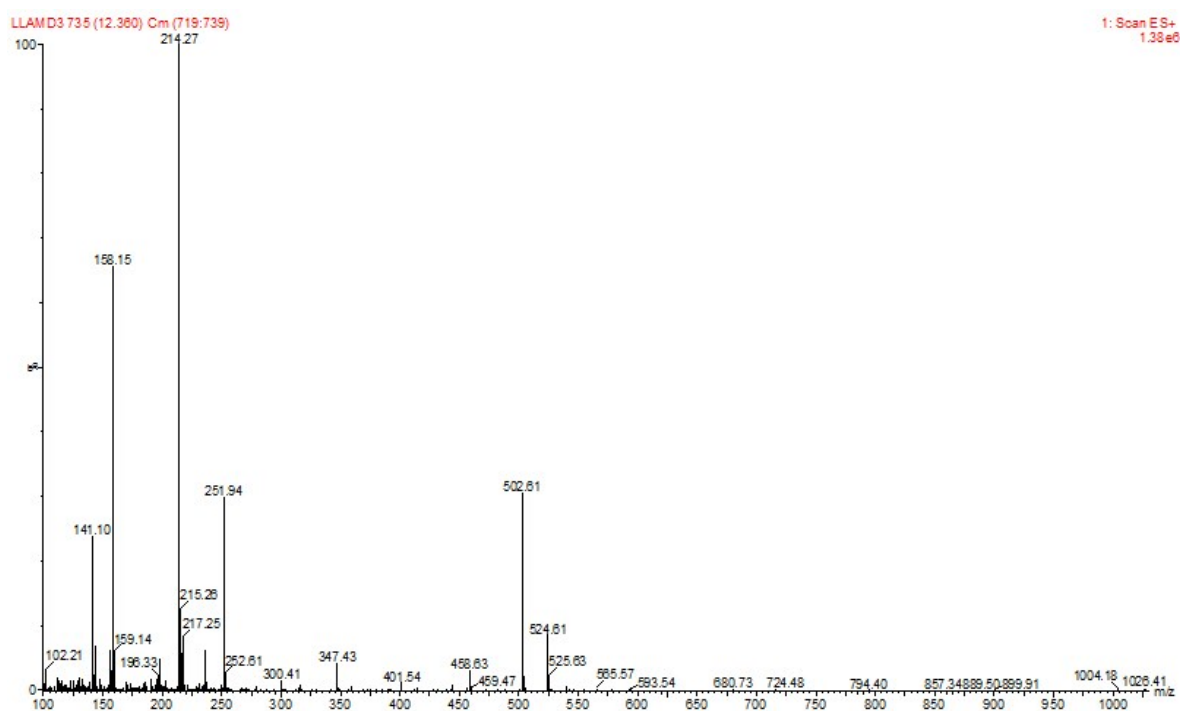


Figure S27b. ESI-MS spectrum of BzHPADO3A, L2



**Figure S28a** HPLC-MS chromatogram of PipHPADO3A, L3



**Figure S28b.** ESI-MS spectrum of PipHPADO3A, L3

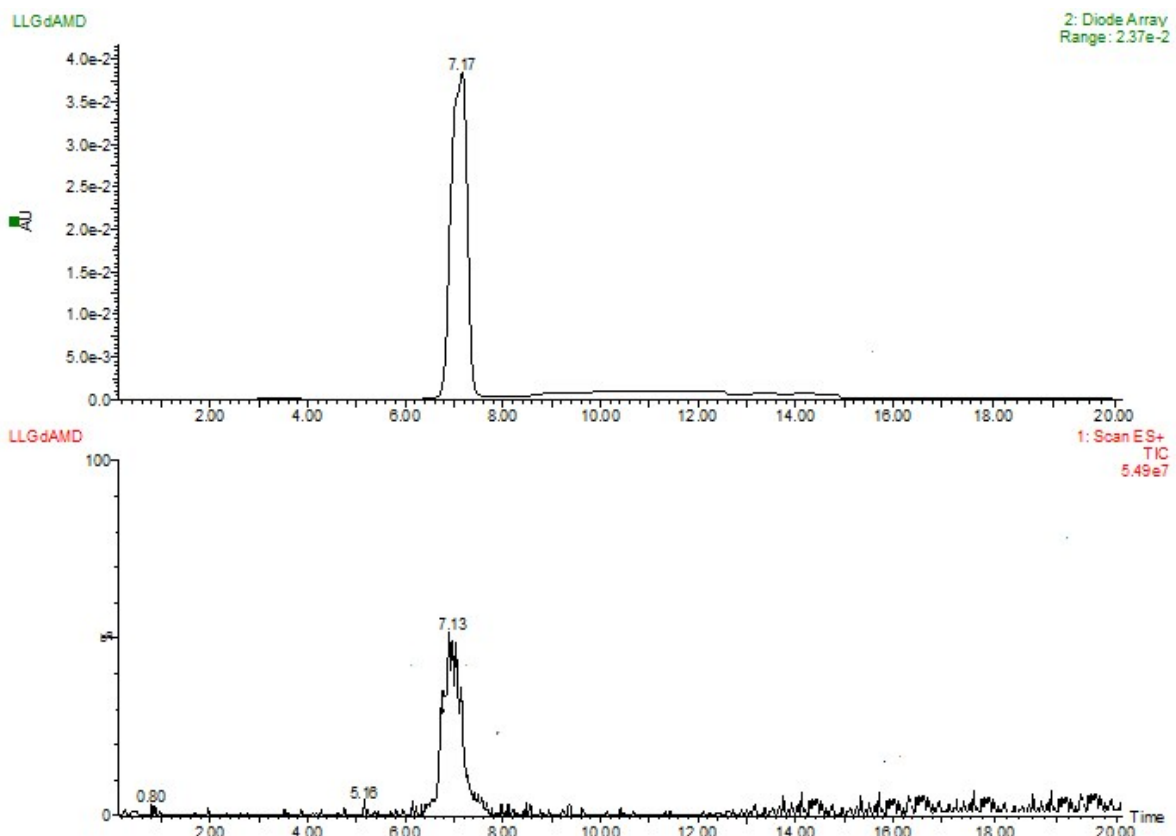
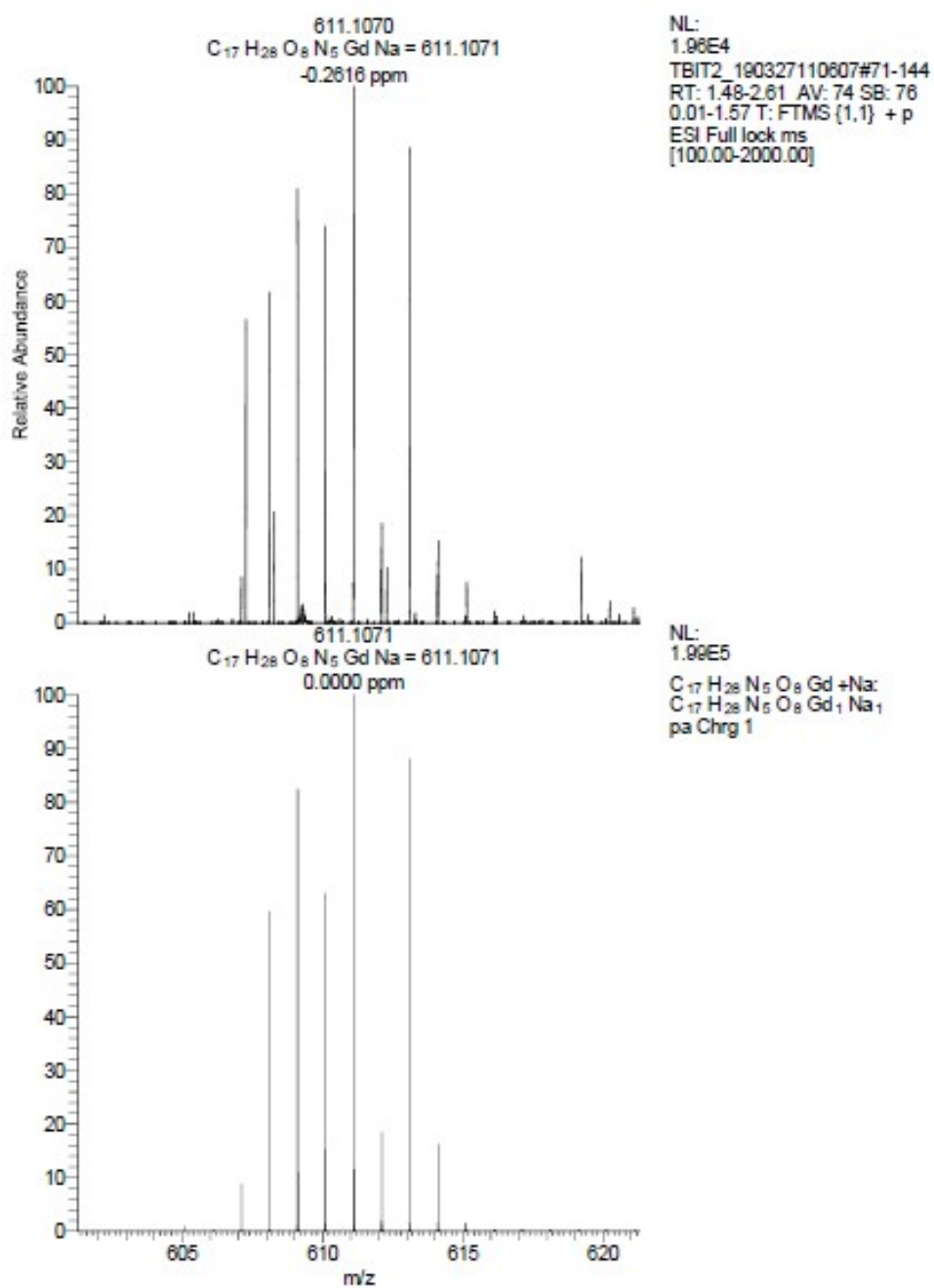
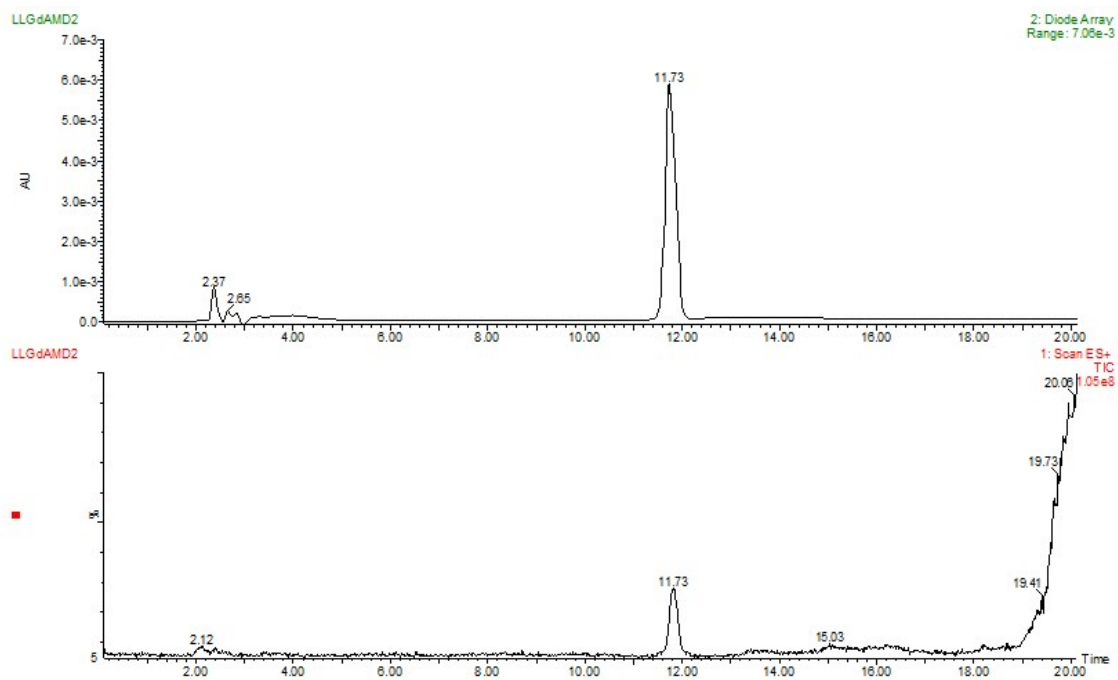


Figure S29a HPLC-MS chromatogram of Gd(HPADO3A), GdL1



**Figure S29b.** Top: high resolution mass spectrum of **Gd(HPADO3A)**, **GdL1**. Below: simulated HRMS for C<sub>17</sub>H<sub>28</sub>GdN<sub>5</sub>NaO<sub>8</sub>



**Figure S30a** HPLC-MS chromatogram of Gd(BzHPADO3A), GdL2

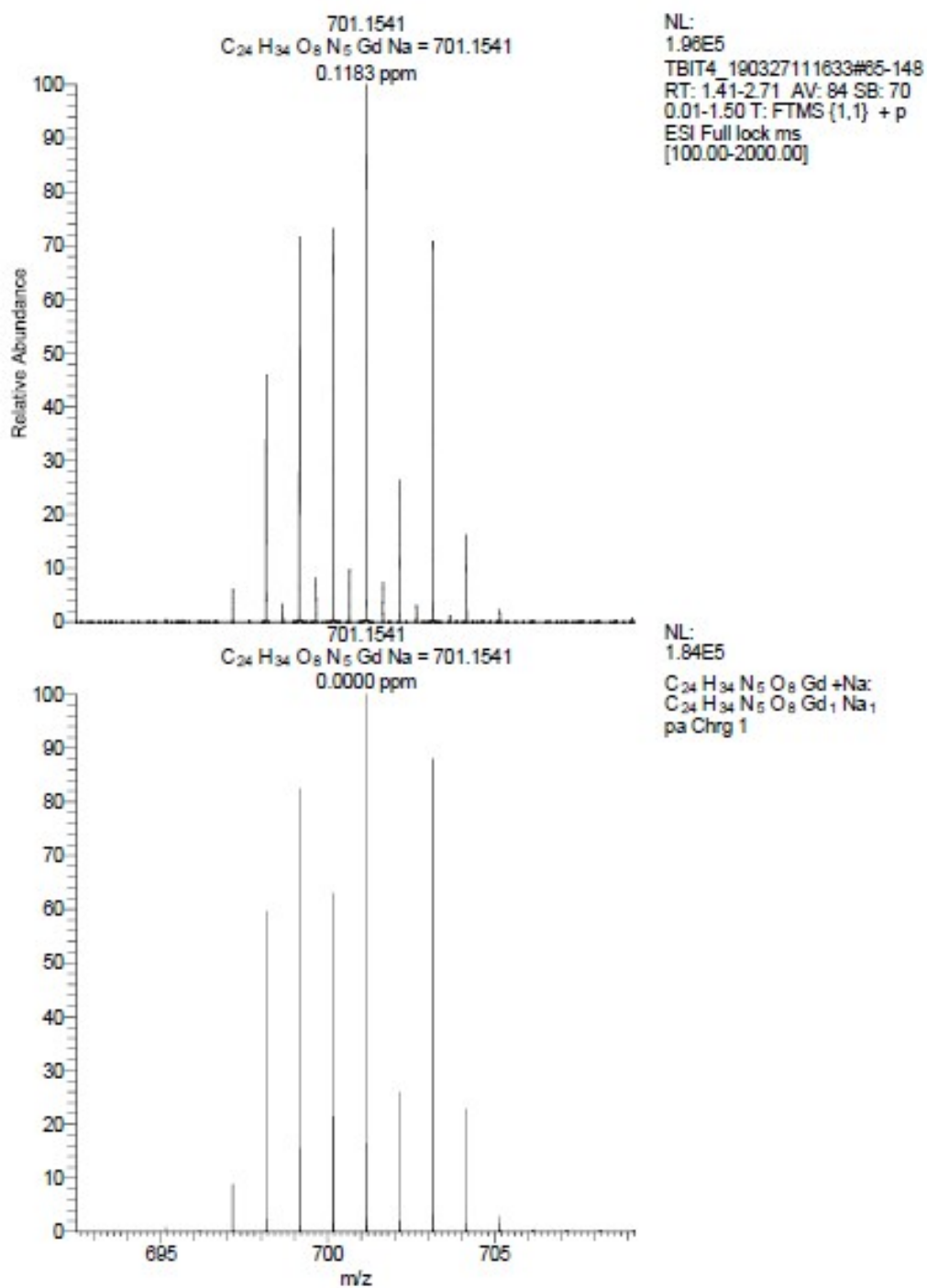
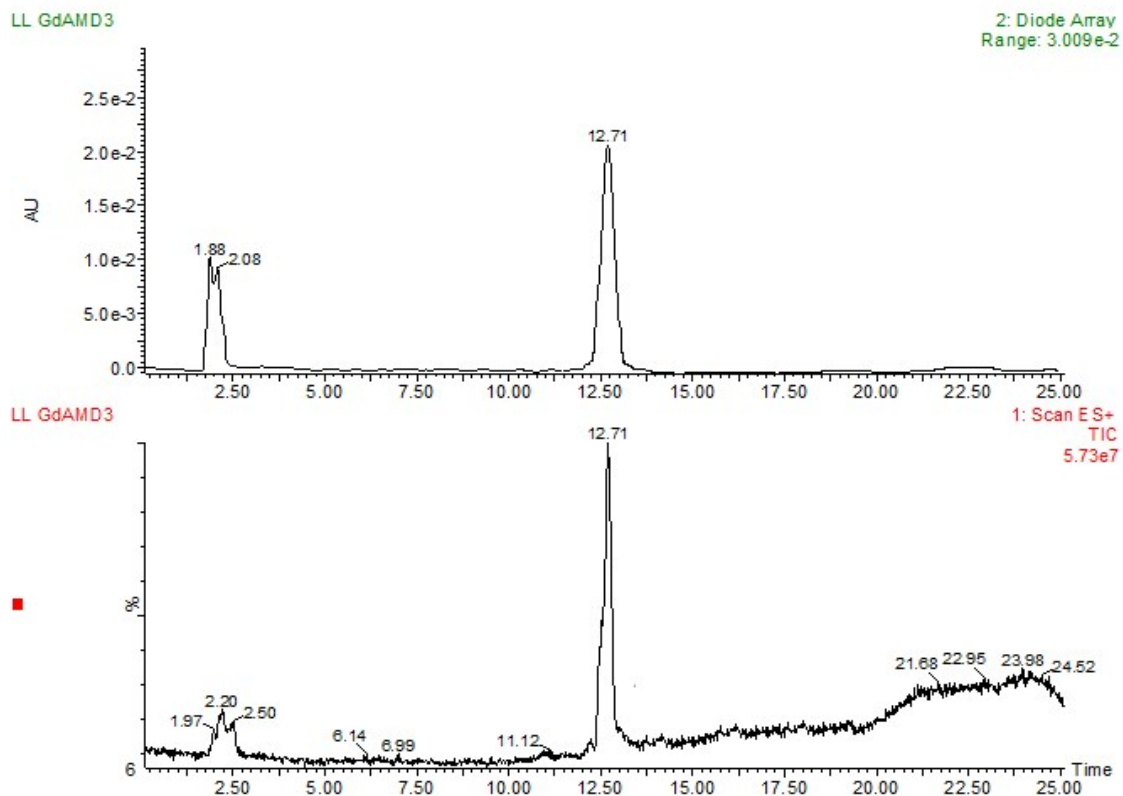
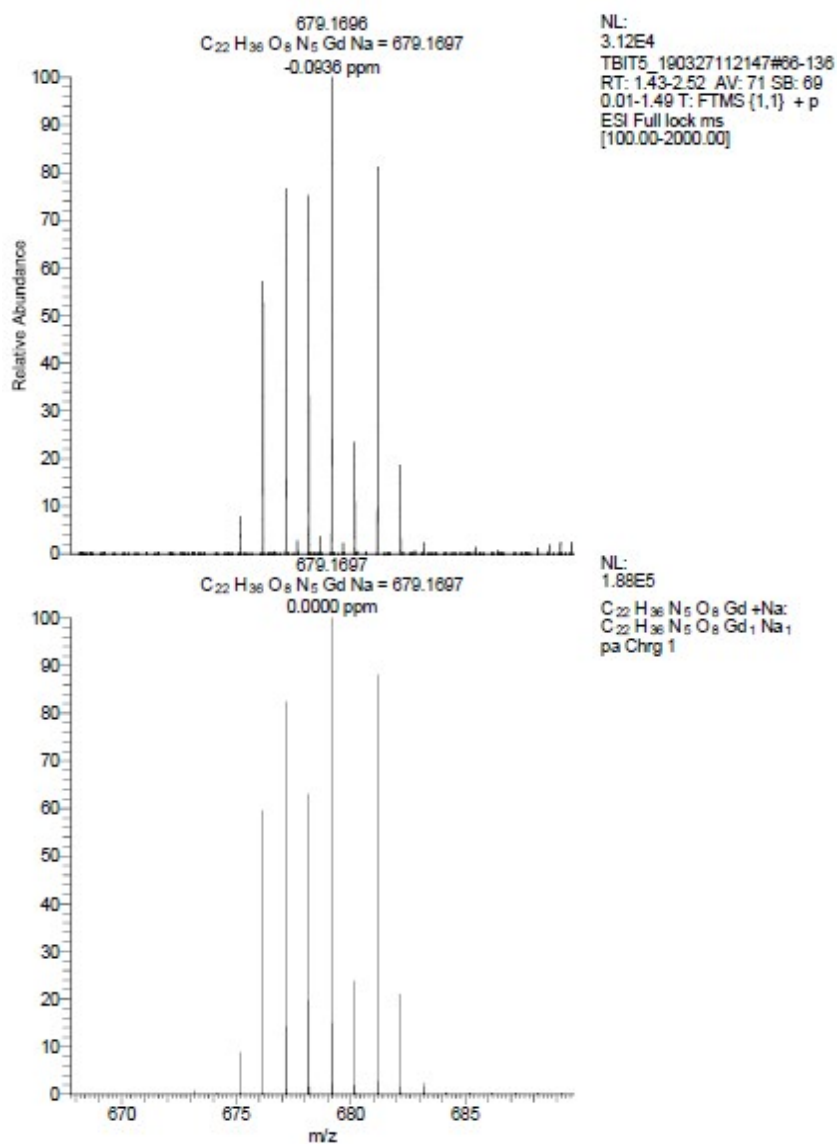


Figure S30b. High resolution mass spectrum of Gd(Bz-HPADO3A), GdL2. Below: simulated HRMS for C<sub>24</sub>H<sub>34</sub>GdN<sub>5</sub>NaO<sub>8</sub>



**Figure S31a** HPLC-MS chromatogram of Gd(PipHPADO3A), GdL3



**Fig. S31b.** High resolution mass spectrum of **Gd(PipHPADO3A)**, **GdL3**. Below: simulated HRMS for C<sub>22</sub>H<sub>36</sub>GdN<sub>5</sub>N

## X. $^1\text{H}$ NMR spectra of EuHPADO3A

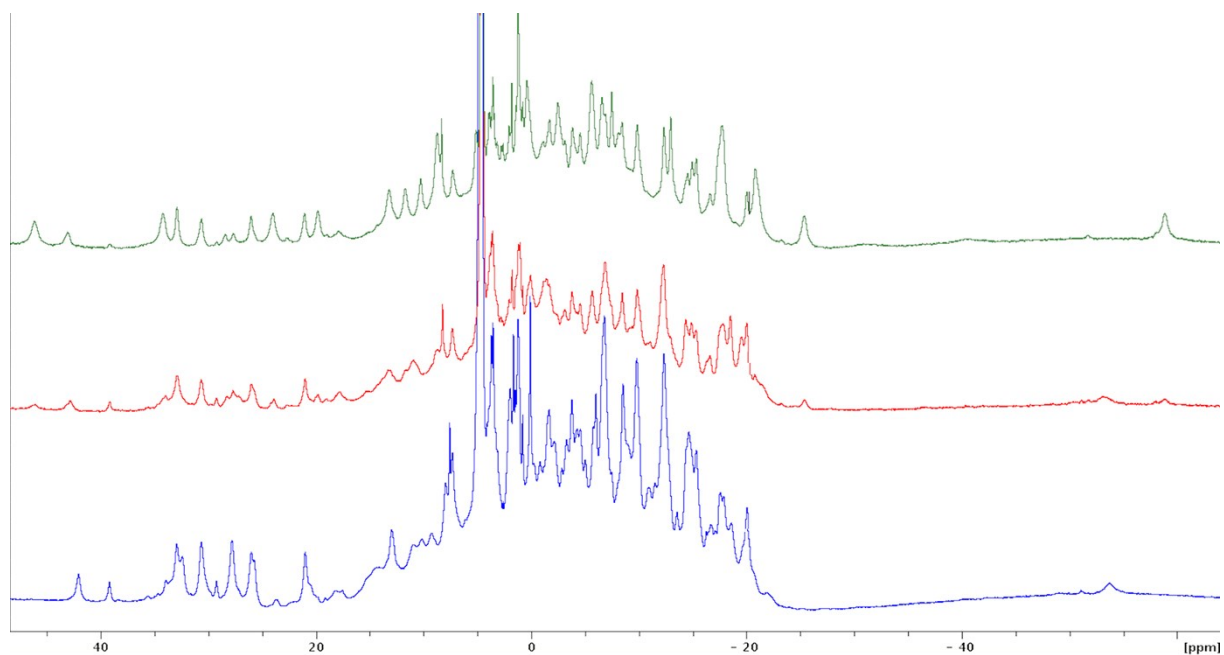


**Fig. S32.**  $^1\text{H}$ -NMR spectra of EuHPADO3A in  $\text{D}_2\text{O}$  at different pD values: 4.2 (below), 7.0 (middle) and 7.6 (top).

The analysis of the  $^1\text{H}$  NMR spectra of Eu(HPA-DO3A) reveals the possible presence of four diastereoisomers due to the presence of the SAP and TSAP coordination isomers and of the R or S configuration on the stereogenic center. Moreover, the analysis of 2D spectra shows that the isomer transition occurs both through the ring and through the arms. We could approximately determine the percentage of the four isomers as 63% for the two SAP isomers and 37% for the two TSAP isomers.

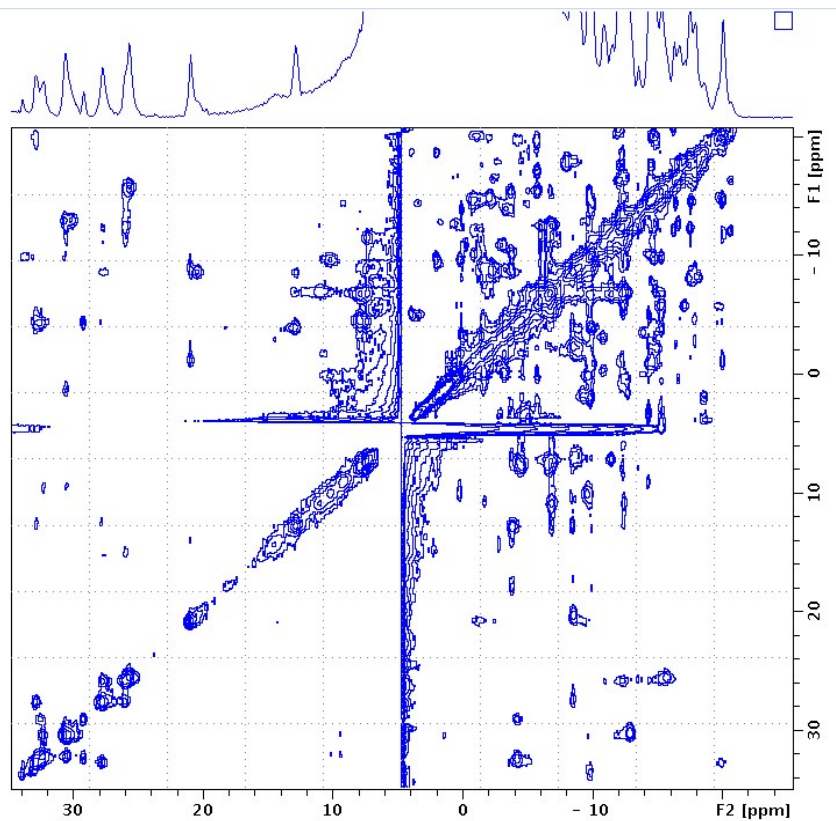


Fig. S33. 2D  $^1\text{H}$ -NMR spectra of EuHPADO3A in  $\text{D}_2\text{O}$  at pD 4.2.

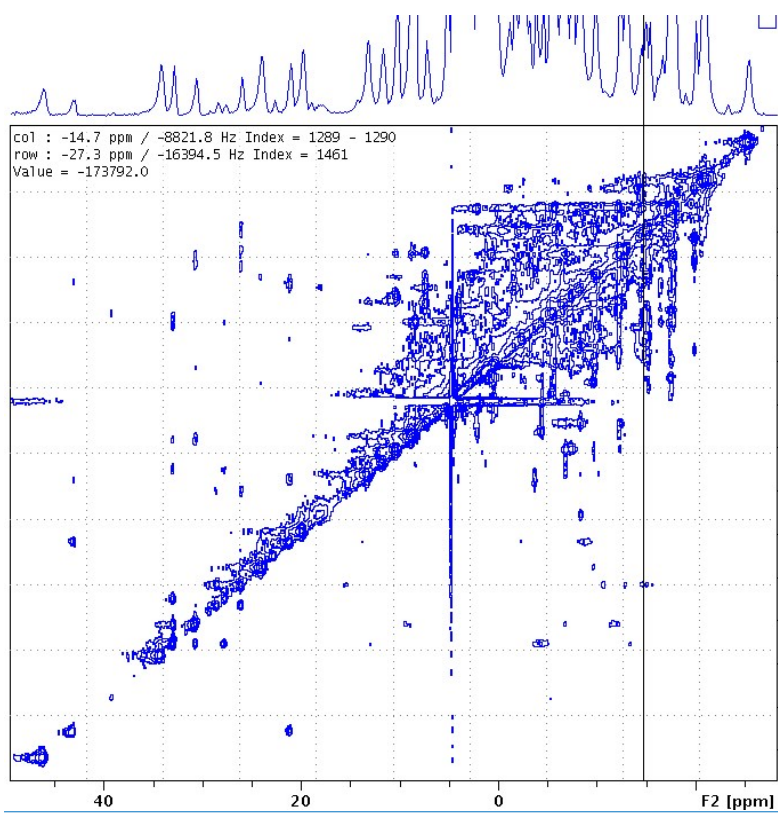


Fig. S34. 2D  $^1\text{H}$ -NMR spectra of EuHPADO3A in  $\text{D}_2\text{O}$  at pD 7.6.